3-6-2024

Depletion of Complement Factor 3 Delays the Neuroinflammatory Response to Intracortical Microelectrodes

Sydney S. Song
Case Western Reserve University, sss176@case.edu

Lindsey N. Druschel
Case Western Reserve University, lnd24@case.edu

Jacob H. Conard
Case Western Reserve University, jhc108@case.edu

Jaime J. Wang
Case Western Reserve University, jjw121@case.edu

Niveda M. Kasthuri
Case Western Reserve University, nmk99@case.edu

See next page for additional authors

Recommended Citation

Sydney S. Song, Lindsey N. Druschel, Jacob H. Conard, Jaime J. Wang, Niveda M. Kasthuri, E. Ricky Chan, Jeffrey R. Capadona, Depletion of complement factor 3 delays the neuroinflammatory response to intracortical microelectrodes. Brain, Behavior, and Immunity, Volume 118, 2024, Pages 221-235. https://doi.org/10.1016/j.bbi.2024.03.004

Brain, Behavior, and Immunity 118 (2024) 221–235

Contents lists available at ScienceDirect

Brain Behavior and Immunity

journal homepage: www.elsevier.com/locate/ybrbi

Full-length Article

Depletion of complement factor 3 delays the neuroinflammatory response to intracortical microelectrodes

Sydney S. Song [a,b], Lindsey N. Druschel [a,b], Jacob H. Conard [a], Jaime J. Wang [a,b], Niveda M. Kasthuri [a,b], E. Ricky Chan [c], Jeffrey R. Capadona [a,b,*]

[a] Department of Biomedical Engineering, Case Western Reserve University, Cleveland, OH 44106, United States
[b] Advanced Platform Technology Center, Louis Stokes Cleveland Veterans Affairs Medical Center, Cleveland, OH 44106, United States
[c] Cleveland Institute for Computational Biology, Case Western Reserve University, Cleveland, OH 44106, United States

ARTICLE INFO

Keywords:
Microelectrode
Inflammation
Complement

ABSTRACT

The neuroinflammatory response to intracortical microelectrodes (IMEs) used with brain-machine interfacing (BMI) applications is regarded as the primary contributor to poor chronic performance. Recent developments in high-plex gene expression technologies have allowed for an evolution in the investigation of individual proteins or genes to be able to identify specific pathways of upregulated genes that may contribute to the neuroinflammatory response. Several key pathways that are upregulated following IME implantation are involved with the complement system. The complement system is part of the innate immune system involved in recognizing and eliminating pathogens – a significant contributor to the foreign body response against biomaterials. Specifically, we have identified Complement 3 (*C3*) as a gene of interest because it is the intersection of several key complement pathways. In this study, we investigated the role of *C3* in the IME inflammatory response by comparing the neuroinflammatory gene expression at the microelectrode implant site between *C3* knockout ($C3^{-/-}$) and wild-type (WT) mice. We have found that, like in WT mice, implantation of intracortical microelectrodes in $C3^{-/-}$ mice yields a dramatic increase in the neuroinflammatory gene expression at all post-surgery time points investigated. However, compared to WT mice, *C3* depletion showed reduced expression of many neuroinflammatory genes pre-surgery and 4 weeks post-surgery. Conversely, depletion of *C3* increased the expression of many neuroinflammatory genes at 8 weeks and 16 weeks post-surgery, compared to WT mice. Our results suggest that *C3* depletion may be a promising therapeutic target for acute, but not chronic, relief of the neuroinflammatory response to IME implantation. Additional compensatory targets may also be required for comprehensive long-term reduction of the neuroinflammatory response for improved intracortical microelectrode performance.

1. Introduction

Intracortical microelectrodes (IMEs) implanted in the cortex of the brain have been widely used to develop brain-machine interfaces (BMIs) because of their ability to record high-resolution neural activity (Hubel, 1957). For example, the recorded neural activity can restore lost function in paralyzed and injured individuals (Fatima et al., 2020; Irwin, 2017; Pandarinath, 2017; Paulk, 2022; Rapeaux and Constandinou, 2021; Simeral, 2011; Willett, 2021). Currently, many neuroscience research studies and clinical applications are under consideration and development in this field (Obien, 2014; Hubel and Wiesel, 1959; Muller, 2015; Stett, 2003; Proix, 2019; Heelan, 2019; Ajiboye, 2017; Jarosiewicz, 2015; Hochberg, 2006; Hochberg and Donoghue, 2006; Khorasani, 2016; Park, 2020; Schroeder and Chestek, 2016). Unfortunately, implantation of IMEs into the brain breaches the blood–brain barrier, damages brain tissue, and initiates a neuroinflammatory cascade (Kozai, 2015; Nolta, 2015; Potter, 2012; Saxena, 2013). The neuroinflammatory response to IMEs persists as long as the device is implanted and is believed to be a major contributing factor to the decline in the quantity and quality of signals obtained (Heelan, 2019).

Many studies have sought to prolong the lifespan of intracortical microelectrodes by targeting these neuroinflammatory pathways. Such

* Corresponding author at: 2071 Martin Luther King Jr. Drive, Room 509, Cleveland, OH 44106, United States.
E-mail addresses: sss176@case.edu (S.S. Song), lnd24@case.edu (L.N. Druschel), jhc108@case.edu (J.H. Conard), jjw121@case.edu (J.J. Wang), nmk99@case.edu (N.M. Kasthuri), erc6@case.edu (E. Ricky Chan), jrc35@case.edu (J.R. Capadona).

https://doi.org/10.1016/j.bbi.2024.03.004
Received 22 November 2023; Received in revised form 26 January 2024; Accepted 2 March 2024
Available online 6 March 2024

approaches include reducing factors that initiate the inflammatory pathways, which includes minimizing the initial trauma associated with device implantation (Shoffstall, 2018; Bjornsson, 2006) and minimizing the chronic mechanical damage caused by device/tissue stiffness mismatch resulting in continuous neuroinflammation (Money, 2020; Bedell, 2018; Nguyen, 2016; Sridharan, 2015; Nguyen, 2014; Harris, 2011; Simon, 2017; Ware, 2012; Welle, 2020). Broadly targeting the inflammatory response with either glucocorticoids such as dexamethasone, anti-inflammatory antibiotics such as minocycline, or antioxidants such as MnTBAP, Dimethyl Fumarate, or resveratrol (Hernandez-Reynoso, 2023; Potter, 2013; Potter-Baker, 2015; Haley, 2020; Kim, 2021; Hoeferlin and T.B., H. Olivares, J. Zhang, L.N. Druschel, B. Sturgill, M. Sobota, P. Boucher, J. Duncan, A.G. Hernandez-Reynoso, S.F. Cogan, J. J. Pancrazio, J.R., 2023) and specific targeting by altering the quantity or function of specific molecules such as laminin, melatonin, flavopiridol, and caspase-1 (Spataro, 2005; Rennaker, 2007; Hermann, 2018; Zhong and Bellamkonda, 2007; He et al., 2006; Golabchi, 2018; Purcell, 2009; Kozai, 2014) have shown promise. Application of extracellular matrix (ECM)-derived compounds that stimulate neuronal growth has also reduced the inflammatory response to microelectrodes (Oakes, 2018; Golabchi, 2020). While these approaches, including broadly immunomodulatory agents, have shown improvements in chronic recordings, long-term application of broad immunomodulatory agents has led to unwanted side effects (Curran, 2022; Heianza, 2020; Kaki, 2011; Buchman, 2001). Immune checkpoint inhibitors such as tislelizumab (which targets the PD-1/PD-L1 complex on T-cells) are used to slow tumor progression but have been shown to cause thyroid dysfunction, pneumonitis, and hyperglycemia (Daei Sorkhabi, 2023; Zhang, 2022). Dexamethazone delivery has been linked to viremia, cardiovascular events, glaucoma, and other adverse side effects throughout the body (Mattos-Silva, 2020; Noreen et al., 2021). Broad immune targeting is also not clinically applicable to patients already susceptible to infection, such as those with spinal cord injuries (Brommer, 2016; Riegger, 2009; Rodgers, 2022; Zhang, 2013). Thus, attenuating the neuroinflammatory pathway through specific molecular targets rather than broad immunomodulation has been explored (Hermann, 2018) with the goal of reducing or circumventing some of the side effects of non-specific therapy. This inspires further investigation into understanding the dynamically changing neuroinflammatory gene expression at the tissue-microelectrode interface in search of targets with minimal off-target effects and maximal immunomodulatory effects.

Utilizing highly parallel gene expression techniques, several labs have investigated the gene expression at the tissue-microelectrode interface (Ereifej, 2018; Bedell, 2020; Song, 2022; Falcone, 2018; Thompson, 2021; Pfluger, 2019; Bennett, 2021), including ours. In past studies, we have investigated the expression of ~ 800 genes in the neuroinflammatory pathway in WT mice and *Cd14* knockout ($Cd14^{-/-}$) mice at acute and chronic time points (Bedell, 2020; Song, 2022; Song, 2023). Hundreds of genes were found to be upregulated at various time points post-surgery, including members of the complement system. At the center of the complement system is *C3*, which several labs have identified as a potentially important and therapeutic target (Bedell, 2020; Song, 2022; Thompson, 2021; Pfluger, 2019; Bennett, 2021), suggesting the need for a detailed investigation into the role of *C3* in microelectrode-induced neuroinflammation.

The complement system is an evolutionarily conserved protein system in innate immunity that helps the host eliminate pathogens and cellular debris (Lubbers, 2017; Nonaka and Yoshizaki, 2004). The complement system forms an activation cascade with three initiating pathways: classical, alternative, and mannose-binding lectin. All initiating paths converge at the level of *C3* amplification. Complement activation results in initiation of the inflammatory process, recruitment of immune cells, lysis of pathogens via the Membrane-Attack Complex (MAC), and opsonization of pathogens to facilitate macrophage phagocytosis (Lubbers, 2017). Unwanted complement system activation significantly contributes to several auto-immune diseases (e.g., hereditary angioedema, paroxysmal nocturnal dyspnea), organ transplant rejection, and foreign body response against biomaterials (Tichaczek-Goska, 2012; Vignesh, 2017; Trouw et al., 2017; Orsini, 2014; Carpanini et al., 2019; Morgan, 2018; Grafals and Thurman, 2019; Mathern and Heeger, 2015; Nilsson, 2007; Ekdahl, 2011).

In this study, we are the first to report the effect of *C3* depletion on the neuroinflammatory response to intracortical microelectrode implantation using $C3^{-/-}$ mice. Here, we examine the expression of 826 neuroinflammatory genes isolated from the tissue-microelectrode interface and surveyed the changes in expression at 4 weeks (4WK), 8 weeks (8WK), and 16 weeks (16WK) post-surgery compared to $C3^{-/-}$ naïve control mice. Additionally, we compare the expression of each of the 826 genes in $C3^{-/-}$ vs WT naïve control, 4WK, 8WK, and 16WK post-surgery time points. Our goal is to evaluate the potential of *C3* as a therapeutic target to reduce microelectrode-induced neuroinflammation and identify genes in the inflammatory pathway that may be targeted synergistically or sequentially with *C3* inhibition.

2. Materials and methods

The materials and methods used in this paper have been routinely performed in our lab, please refer to (Bedell, 2020); (Song, 2022), and (Song, 2023) for more details. Briefly:

Animals and surgical procedures: A total of 20 male C57BL/6J $C3^{-/-}$ (Jackson Laboratory Strain #003641) mice and 20 male C57BL/6J WT mice (Jackson Laboratory Strain #000664) were used in this study. Both WT and C57BL/6J $C3^{-/-}$ mice were randomly divided into 4 groups of 5 animals each: naïve control, and 4 weeks, 8 weeks, and 16 weeks post-surgery. Animals were implanted with "dummy probes" in the shape of Michigan-style silicon microelectrodes. Probes were 2 mm long, 123 μm wide at the widest portion of the shank, and 15 μm thick. These probes were graciously provided by the Pancrazio Lab at the University of Texas at Dallas. A total of 4 probes were implanted 1.5 mm both left and right lateral of midline and 1.0 mm both anterior/posterior to the bregma for each mouse. For a comprehensive description of surgical protocols, see (Song, 2023; Ereifej, 2018; Ravikumar, 2014; Ravikumar, 2014). Prior to implantation, dummy probes were washed by soaking in 95 % ethanol solution three times for 5 min each and sterilized with cold ethylene oxide gas following established protocols. All animal care and handling were performed in compliance with a protocol approved by the Institutional Animal Care and Use Committee (IACUC) at Case Western Reserve University.

Tissue Extraction: At predefined end time points, anesthetized mice (100 mg/kg ketamine and 10 mg/kg xylazine) were euthanized via cardiac perfusions with ~ 50–100 mL cold 1X phosphate-buffered saline (PBS). Mouse brains were immediately extracted to prevent excessive RNA degradation. Probes were removed prior to the brains undergoing flash freezing in optimal cutting temperature compound (OCT), and storage at −80 °C until cryosection. Three to four 150 μm slices were obtained for bulk gene expression analysis, and approximately twenty-five 5 μm slices were obtained for use in another project. The top 50–100 μm of the brain was excluded to ensure slices were taken from the same depth of the cortex for all four implants, this accounts for any slight variations in the angle of the brain in the OCT. The remaining depth of 700–900 μm of cortical tissue was sliced. From the 150 μm slices, tissue within a 500 μm radius of the implantation site was excised with a biopsy punch (1 mm diameter).

RNA Isolation: Brain tissue biopsies were homogenized with the Bead Bug Homogenizer (Benchmark Scientific D1030) and RNA was extracted and purified with RNeasy® Plus Universal Mini Kit (Qiagen 73404) at the Gene Expression and Genotyping Facility at Case Western Reserve University (Bedell, 2020; Song, 2023).

Gene Expression Assay: Full details can be found in our earlier publications (Song, 2023; Song and H.W.B., B.J. Regan, E.S. Ereifej, R. Chan, J.R. Capadona, 2022). RNA was processed according to manufacturer protocols (Neuroinflammatory Panel, NanoString Technologies,

Seattle, WA) and read via nCounter® Max Analyzer at 280 Field-of-View per sample. Here, we used a codeset containing 826 genes: 773 were from the nCounter® Mouse Neuroinflammation Panel (shown in black), which included 13 housekeeping genes (shown in blue with dark gray shading), and 53 custom genes of interest (shown in red with light gray shading) (Table 1). Custom genes included oxidative stress markers, additional complement genes, and other pathways for neuroinflammation. Additionally, both positive and negative controls were spiked in as quality control for all experiments.

3. Data visualization and statistical analysis

Exclusion, normalization, and statistical analyses were all performed in nSolver 4.0 and Advanced Analysis 4.0 (NanoString Technologies, Seattle, WA).

Exclusion criteria: Genes with counts below 25 in 85 % of the total samples, and housekeeping genes (HK) with average raw counts below 75.

Normalization: Raw counts for each sample were normalized to the geometric mean of spiked-in positive controls and to the geometric mean of HK controls.

Statistical Significance: An unpaired T-test with a Benjamini-Hochberg False-Discovery-Rate Correction was used to calculate adjusted p-values (p_{adj}) and significance was set at $p_{adj} < 0.05$ (Bedell, 2020).

Data Visualization: Gene expression is summarized for each comparison using volcano plots created with GraphPad Prism 10. Volcano plots have one point for every gene measured in that experiment, with log2(fold change) on the x-axis, and $-\log10(p_{adj})$ on the y-axis. Fold change is equal to the average expression of the experimental group divided by the average expression of the control (or baseline) group. If the experimental group has higher expression of a particular gene, then the ratio of experimental expression to control expression will be greater than 1, making the log base 2 of that ratio positive. This means the point for that specific gene will lie in the right side of the y-axis. In the $C3^{-/-}$ implanted vs. un-implanted $C3^{-/-}$ comparison, the control group will always be naïve control $C3^{-/-}$ mice with no implant. In the implanted WT vs. implanted $C3^{-/-}$ comparisons, the control group is the implanted WT mice, meaning all points to the left of the y-axis represent genes that are higher expressed in WT mice compared to $C3^{-/-}$ mice. On the y-axis, the significance cutoff of $p_{adj} = 0.05$ corresponds to points above $-\log10(p_{adj}) = 1.30$, and the higher the point is located on the plot, the smaller the P-value. (Bedell, 2020).

Gene and Pathway Analysis: Advaita iPathwayGuide was used to help understand the different roles specific genes play in the body (Draghici, 2007; Donato, 2013). Gene name, Log2FoldChange, and p_{adj} were input into the software, which generates a detailed analysis report. We utilized 3 specific functions focusing on pathways, biological processes, and molecular components. The pathway analysis searches all known Kyoto Encyclopedia of Genes and Genomes (KEGG) pathways involved in the differentially expressed genes and allows us to see possible downstream effects for genes that were differentially expressed (Kanehisa and Goto, 2000; Kanehisa, 2019; Kanehisa, 2023). Diagrams from the KEGG database are included for each of the pathways discussed, though several are in supplementary. The biological processes and molecular components functions allow us to see what processes and structures that the genes will impact, even if the specific pathways aren't fully known or understood. These functions use gene ontology (GO) terms to group specific processes and components (Ashburner, 2000; Gene Ontology, 2023). We examined the results from these 3 features to discern how these genes contribute to the inflammatory response of IME implantation.

4. Results

Neuroinflammatory gene expression following IME implantation in $C3^{-/-}$ mice compared to $C3^{-/-}$ Naïve Control

We first examined the gene expression of 826 genes in the neuroinflammatory pathway within 500 μm of the microelectrode-tissue interface in $C3^{-/-}$ mice at 4WK, 8WK, and 16WK post-surgery. All gene expression in surgical $C3^{-/-}$ mice were compared to naïve, non-surgical control $C3^{-/-}$ mice to evaluate how the expression of genes in $C3^{-/-}$ neuroinflammatory pathways change following microelectrode implantation. Of the 826 genes measured, 529 were found to be significantly differentially expressed in at least 1 comparison (Fig. 1). The remaining 297 quantified genes that we included showed no changes in expression level above p_{adj} threshold < 0.05 in any comparison. Fig. 1**A** displays a Venn diagram indicating the number of differentially expressed genes post-surgery in $C3^{-/-}$ implaned mice compared to $C3^{-/-}$ naïve control mice for each of the three time points we examined. Genes were included if $p_{adj} < 0.05$. Overlapping spaces in the diagram indicate that the same genes demonstrated differential expression across multiple timepoints. Supplementary Table S1 lists the genes that were significantly upregulated or downregulated at each time point post-surgery.

At 4WK post-surgery, a total of 41 genes showed changes in expression with statistical significance ($p_{adj} < 0.05$) (Fig. 1A, 1B, and Table S1). Four of these genes: *Dcx, Ptgs2, Nlrp2,* and *Npnt* showed downregulation, while the remaining 37 genes all showed upregulation. *Dcx,* which codes for the doublecortin protein, is a cytoplasmic neuronal protein that contributes to microtubule networks. *Ptgs2* is a gene that codes for the cyclooxygenase 2 protein, which is involved in both synaptic activity and enzymatic synthesis of pro-inflammatory factors (L., m., 2004; Rawat and S.K., U. Ranjan Dahiya, R. Kukreti, 2019). *Nlrp2*, or NLR family, pyrin domain containing 2, is a gene expressed in astrocytic inflammasomes (Minkiewicz and J.P.d.R.V., Robert W. Keane, 2013). Nephronectin, encoded by the gene *Npnt*, is an extracellular matrix protein that is involved in cell–cell adhesion. *Dcx, Ptgs2, and Npnt* are likely downregulated because they all have roles in maintaining the structure of neural cells, which is disrupted following IME implantation. *Nlrp2*, however, is an interesting gene to be downregulated, as its downregulation suggests that this type of astrocytic inflammasome is not being utilized to respond to the implantation of the electrode. Rather, other lysosomes and phagosomes are overtaking that role, which was evident in the pathway analysis. The pathways found to be upregulated in the 4WK implanted animals are associated mainly with the brain's foreign body response, including phagosome formation (*Clec7a, Cd36, Fcgr2b, Fcgr3, Tclrg1,* KEGG:04145), antigen processing and presentation (*Cd74, Ctss, Ifi30,* KEGG:04612), and lysosome formation (*Ctss, Cd68, Tclrg1,* KEGG:04142) (Fig. 2).

Of the 37 genes that were differentially upregulated at the 4WK time point, 36 were found to remain upregulated through 8WK post-surgery time point (Fig. 1A, C, and Table S1). One gene, *Anxa1*, was upregulated in the 4WK and 16WK time points, but was not differentially expressed at the 8WK time point. *Anxa1* is a gene that has an anti-inflammatory role in the peripheral nervous system and promotes BBB integrity in the central nervous system (McArthur, 2016). The phagosome, antigen processing, and lysosome associated pathways upregulated in the 4WK timepoint remain activated into the 8WK time point. However, at 8WK post-surgery, another 323 genes were upregulated in the implanted animals (Fig. 1A, C, and Table S1). No genes are downregulated in the 8WK time point. At 8WK, we see the onset of several key inflammatory signaling pathways, including NOD-like receptor (KEGG:04621, Supplemental Fig. S2A), MAPK (KEGG:04010, Supplemental Fig. S2B), toll-like receptor (KEGG:04620, Supplemental Fig. S2C), and p53 (KEGG:04115, Supplemental Fig. S2D). These pathways often activate one another and are highly intertwined. For instance, toll-like receptor pathway genes (*Myd88, Irak4, Irf3, Traf6, Irak1*) activate NOD-like or MAPK receptor pathways (Supplemental Fig. S2A-C). Certain NOD-like receptor signaling pathway genes *(Xiap, Traf, Ripk2)* activate pro-inflammatory cascades in the MAPK signaling pathways, and MAPK genes (*Mapk14*, *Map3k1*, *Map2k4*) activate p53 signaling (Supplemental Fig. S2B). The common effects of these pathways include the release of pro-inflammatory cytokines and chemokines as well as apoptosis. Many

Table 1
Complete list of neuroinflammatory genes of interest utilized in this study. Here we list the 826 genes examined in the current study. Genes from the nCounter® Mouse Neuroinflammation Panel (shown in black), the 53 custom genes of interest are in red (light gray shading), and 13 housekeeping genes are in blue (dark gray shading).

Abcc3	Bok	Cd8a	Ddb2	Foxp3	Igsf10	Kir3dl2	Mmp14	Parp1	Rad51c	Smarca4	Tnfrsf13c
Abcc8	Bola2	Cd8b1	Ddx58	Fpr1	Igsf6	Kit	Mmp16	Parp2	Rad9a	Smarca5	Tnfrsf17
Abl1	Braf	Cdc25a	Dicer1	Fscn1	Ikbkb	Klrb1	Mmp19	Pcna	Rag1	Smarcd1	Tnfrsf1a
Adamts13	Brca1	Cdc7	Dlg1	Fyn	Ikbke	Klrd1	Mmp2	Pdpn	Rala	Smc1a	Tnfrsf1b
Adamts16	Brd2	Cdk20	Dlg4	Gadd45a	Ikbkg	Klrk1	Mmp24	Pecam1	Ralb	Snca	Tnfrsf25
Ago4	Brd3	Cdkn1a	Dlx1	Gadd45g	Il10	Kmt2a	Mmp9	Pex14	Rapgef3	Socs3	Tnfrsf4
Agt	Brd4	Cdkn1c	Dlx2	Gal3st1	Il10rb	Kmt2c	Mobp	Pik3ca	Rb1cc1	Sod1	Tnfsf10
AI464131	Btk	Ceacam3	Dna2	Gba	Il15ra	Lacc1	Mog	Pik3cb	Rbfox3	Sod2	Tnfsf12
Aim2	C1qa	Cfb	Dnmt1	Gbp2	Il1a	Lag3	Mok	Pik3cd	Rela	Sod3	Tnfsf13b
Ak1	C1qb	Cfh	Dnmt3a	Gclc	Il1b	Lair1	Mpeg1	Pik3cg	Relb	Sox10	Tnfsf4
Akt1	C1qc	Cfi	Dnmt3b	Gdpd2	Il1f5	Lama1	Mpg	Pik3r1	Reln	Sox4	Tnfsf8
Akt2	C3	Cflar	Dock1	Gfap	Il1r1	Lamb1	Mr1	Pik3r2	Reserved	Sox9	Top2a
Aldh1l1	C3ar1	Ch25h	Dock2	Gja1	Il1r2	Lamb2	Mre11a	Pik3r5	Rgl1	Sphk1	Topbp1
Ambra1	C4a	Chek1	Dot1l	Gjb1	Il1rap	Lamp1	Ms4a1	Pilra	Rhoa	Spib	Tpd52
Amigo2	C4bp	Chek2	Dst	Gna15	Il1rl2	Lamp2	Ms4a2	Pilrb1	Ripk1	Spint1	Tpsb2
Anapc15	C5ar1	Chn2	Duoxa1	Gpr183	Il1rn	Lcn2	Ms4a4a	Pink1	Ripk2	Spp1	Tradd
Anxa1	C6	Chst8	Dusp7	Gpr34	Il21r	Ldha	Msh2	Pla2g4a	Rnf8	Sqstm1	Traf1
Apc	C7	Chuk	E2f1	Gpr62	Il2rg	Ldlrad3	Msn	Pla2g5	Robo3	Srgn	Traf2
Apex1	C9	Cidea	Eed	Gpr84	Il3	Lfng	Msr1	Plcg2	Rpa1	Srxn1	Traf3
Apoe	Cables1	Cideb	Eef2k	Grap	Il3ra	Lgmn	Mvp	Pld1	Rpl28	St3gal6	Traf6
App	Calcoco2	Cks1b	Egfr	Gria1	Il6	Lig1	Myc	Pld2	Rpl29	St8sia6	Trat1
Aqp4	Calr	Clcf1	Egr1	Gria2	Il6ra	Lilrb4a	Myct1	Plekhb1	Rpl36al	Stat1	Trem1
Arc	Camk4	Cldn5	Ehd2	Gria4	iNos	Lingo1	Myd88	Plekhm1	Rpl9	Steap4	Trem2
Arg1	Casp1	Clec4e	Ehmt2	Grin2a	Inpp5d	Lmna	Myrf	Pllp	Rps10	Stmn1	Trem3
Arhgap24	Casp2	Clec7a	Eif1	Grin2b	Iqsec1	Lmnb1	Nbn	Plp1	Rps2	Stx18	Trim47
Arid1a	Casp3	Clic4	Emcn	Grm2	Irak1	Lrg1	Ncaph	Plxdc2	Rps21	Sumo1	Trp53
Asb2	Casp4	Cln3	Emp1	Grm3	Irak2	Lrrc25	Ncf1	Plxnb3	Rps3	Suv39h1	Trp53bp2
Ash2l	Casp6	Clstn1	eNos	Grn	Irak3	Lrrc3	Ncor1	Pmp22	Rps9	Suv39h2	Trp73
Asph	Casp7	Clu	Enpp6	Gsn	Irak4	Lsr	Ncor2	Pms2	Rrm2	Suz12	Trpa1
Atf3	Casp8	Cnn2	Entpd2	Gstm1	Irf1	Lst1	Ncr1	Pnoc	Rsad2	Syk	Trpm4
Atg14	Casp9	Cnp	Eomes	Gzma	Irf2	Lta	Nefl	Pole	Rtn4rl1	Syn2	Tspan18
Atg3	Cass4	Cntnap2	Ep300	Gzmb	Irf3	Ltb	Nfe2l2	Ppfia4	S100a10	Syp	Ttr
Atg5	Ccl2	Coa5	Epcam	H2afx	Irf4	Ltbr	Nfkb1	Ppp3ca	S100b	Tarbp2	Tubb3
Atg7	Ccl3	Col1a1	Epg5	H2-T23	Irf6	Ltc4s	Nfkb2	Ppp3cb	S1pr3	Tbc1d4	Tubb4a
Atg9a	Ccl4	Col3a1	Epsti1	Hat1	Irf7	Ly6a	Nfkbia	Ppp3r1	S1pr4	Tbr1	Txnrd1
Atm	Ccl5	Col4a1	Erbb3	Hc	Irf8	Ly6g	Nfkbie	Ppp3r2	S1pr5	Tbx21	Tyrobp
Atp6v0e	Ccl7	Col6a3	Ercc2	Hcar2	Islr2	Ly9	Ngf	Prdx1	Sall1	Tcirg1	Ugt8a
Atp6v1a	Ccng2	Cotl1	Ercc6	Hdac1	Itga6	Lyn	Ngfr	Prf1	Scd1	Tcl1	Ulk1
Atr	Ccni	Cox5b	Esam	Hdac2	Itga7	Mafb	Ninj2	Prkaca	Sell	Tet1	Ung
Axl	Ccr2	Cp	Ets2	Hdac4	Itgam	Maff	Nkg7	Prkacb	Serpina3n	Tfg	Uty

(continued on next page)

Table 1 (*continued*)

B3gnt5	Ccr5	Cpa3	Exo1	Hdac6	Itgav	Mag	Nlgn1	Prkar1a	Serpine1	Tgfa	Vamp7
Bad	Cd109	Cr2	Ezh1	Hdc	Itgax	Mal	Nlgn2	Prkar2a	Serpinf1	Tgfb1	Vav1
Bag3	Cd14	Creb1	Ezh2	Hells	Itgb5	Man2b1	Nlrp2	Prkar2b	Serping1	Tgfbr1	Vegfa
Bag4	Cd163	Crebbp	F3	Hif1a	Jag1	Map1lc3a	Nlrp3	Prkce	Sesn1	Tgm1	Vim
Bak1	Cd19	Crem	Fa2h	Hilpda	Jam2	Map2	nNos	Prkcq	Sesn2	Tgm2	Vps4a
Bard1	Cd209e	Crip1	Fabp5	Hira	Jarid2	Map2k1	Nod1	Prkdc	Setd1a	Thbd	Vps4b
Bax	Cd244	Cryba4	Fadd	Hist1h1d	Jun	Map2k4	Nostrin	Prnp	Setd1b	Tie1	Vtn
Bbc3	Cd24a	Csf1	Fancc	Hmgb1	Kat2a	Map3k1	Noxa1	Pros1	Setd2	Timeless	Was
Bcas1	Cd300lf	Csf1r	Fancd2	Hmox1	Kat2b	Map3k14	Npl	Psen2	Setd7	Timp1	Wdr5
Bcl10	Cd33	Csf2rb	Fancg	Homer1	Kcnd1	Mapk10	Npnt	Psmb8	Setdb1	Tle3	Xcl1
Bcl2	Cd36	Csf3r	Fas	Hpgds	Kcnj10	Mapk12	Nptx1	Pten	Sftpd	Tlr2	Xiap
Bcl2a1a	Cd3d	Csk	Fasl	Hprt	Kcnk13	Mapk14	Nqo1	Ptger3	Sh2d1a	Tlr4	Xrcc6
Bcl2l1	Cd3e	Cspg4	Fbln5	Hps4	Kdm1a	Mapt	Nrgn	Ptger4	Shank3	Tlr7	Zbp1
Bcl2l11	Cd3g	Cst7	Fcer1g	Hrk	Kdm1b	Marco	Nrm	Ptgs2	Siglec1	Tm4sf1	Zfp367
Bcl2l2	Cd40	Ctse	Fcgr1	Hsd11b1	Kdm2a	Mavs	Nrp2	Ptms	Siglecf	Tmc7	Aars
Bdnf	Cd44	Ctsf	Fcgr2b	Hspb1	Kdm2b	Mb21d1	Nthl1	Ptpn6	Sin3a	Tmcc3	Asb10
Becn1	Cd46	Ctss	Fcgr3	Hus1	Kdm3a	Mbd2	Nwd1	Ptprc	Sirt1	Tmem100	Ccdc127
Bid	Cd47	Ctsw	Fcrla	Icam2	Kdm3b	Mbd3	Oas1g	Pttg1	Slamf8	Tmem119	Cnot10
Bik	Cd55b	Cx3cl1	Fcrlb	Ifi30	Kdm4a	Mbl2	Ogg1	Ptx3	Slamf9	Tmem144	Csnk2a2
Bin1	Cd59a	Cx3cr1	Fcrls	Ifih1	Kdm4b	Mcm2	Olfml3	Pycard	Slc10a6	Tmem173	Fam104a
Birc2	Cd6	Cxcl10	Fdxr	Ifitm2	Kdm4c	Mcm5	Opalin	Rab6b	Slc17a6	Tmem204	Gusb
Birc3	Cd68	Cxcl9	Fen1	Ifitm3	Kdm4d	Mcm6	Optn	Rab7	Slc17a7	Tmem206	Lars
Birc5	Cd69	Cycs	Fgd2	Ifna1	Kdm5a	Mdc1	Osgin1	Rac1	Slc1a3	Tmem37	Mto1
Blk	Cd70	Cyp27a1	Fgf13	Ifnar1	Kdm5b	Mdm2	Osmr	Rac2	Slc2a1	Tmem64	Supt7l
Blm	Cd72	Cyp7b1	Fgl2	Ifnar2	Kdm5c	Mef2c	P2rx7	Rad1	Slc2a5	Tmem88b	Tada2b
Blnk	Cd74	Cytip	Fkbp5	Ifng	Kdm5d	Mertk	P2ry12	Rad17	Slc44a1	Tnf	Tbp
Bmi1	Cd83	Dab2	Flt1	Igf1	Kdm6a	Mfge8	Pacsin1	Rad50	Slc6a1	Tnfrsf10b	Xpnpep1
Bnip3	Cd84	Dapk1	Fn1	Igf1r	Kif2c	Mgmt	Padi2	Rad51	Slco2b1	Tnfrsf11b	
Bnip3l	Cd86	Dcx	Fos	Igf2r	Kir3dl1	Mmp12	Pak1	Rad51b	Slfn8	Tnfrsf12a	

genes in the mouse apoptosis pathway (Supplemental Fig. S3, 26 total, including *Lmna, Parp1,* and *Bcl2)* are upregulated at the 8WK timepoint, demonstrating that these inflammatory pathways are inducing downstream effects and killing local cells.

By the 16WK post-surgery time point, there is the largest upregulation of inflammatory genes. Thirty-five of the genes upregulated at both 4WK and 8WK maintained upregulation through 16WK post-surgery (Fig. 1A). These genes include mainly the phagosome (Supplemental Fig. S4A), antigen processing (Supplemental Fig. S4B), and lysosome pathways (Supplemental Fig. S4C), which have continuously been upregulated since the acute 4WK timepoint (Fig. 2). Additionally, 349 of the 359 genes showing upregulation at 8WK post-surgery remained upregulated at 16WK post-surgery (Fig. 1A, 1C, 1D and Table S1). One gene, *Ccl5*, was upregulated in the 4WK and 8WK timepoints but returned to baseline by 16WK. *Ccl5* is expressed by microglia and astrocytes and acts as a chemoattractant for immune cells to cross the BBB (Bayly-Jones, 2020). At 16WK post-surgery, 515 genes showed upregulation with statistical significance ($p_{adj} < 0.05$), including 165 newly upregulated genes (Figs. 1, 1D and Table S1). Of these 165, 30 were associated with neurodegeneration and apoptosis (Supplemental Fig. S5), and 41 were involved in the signaling pathways discussed previously in the 8WK section (Supplemental Fig. S2): NOD-like receptor (Supplemental Fig. S6A), MAPK (Supplemental Fig. S6B), toll-like receptor (Supplemental Fig. S6C), and p53 (Supplemental Fig. S6D). We also see an increase in the following pathways: axon guidance (KEGG:04360, Supplemental Fig. S7A; 15 genes), Ras signaling (KEGG:04014, Supplemental Fig. S7B; 41 genes), Rap1 signaling (KEGG:04015, Supplemental Fig. S7C; 27 genes), and ErbB signaling (KEGG:04012, Supplemental Fig. S7D; 21 genes), all of which are involved with cell adhesion, extension, or remodeling. All these

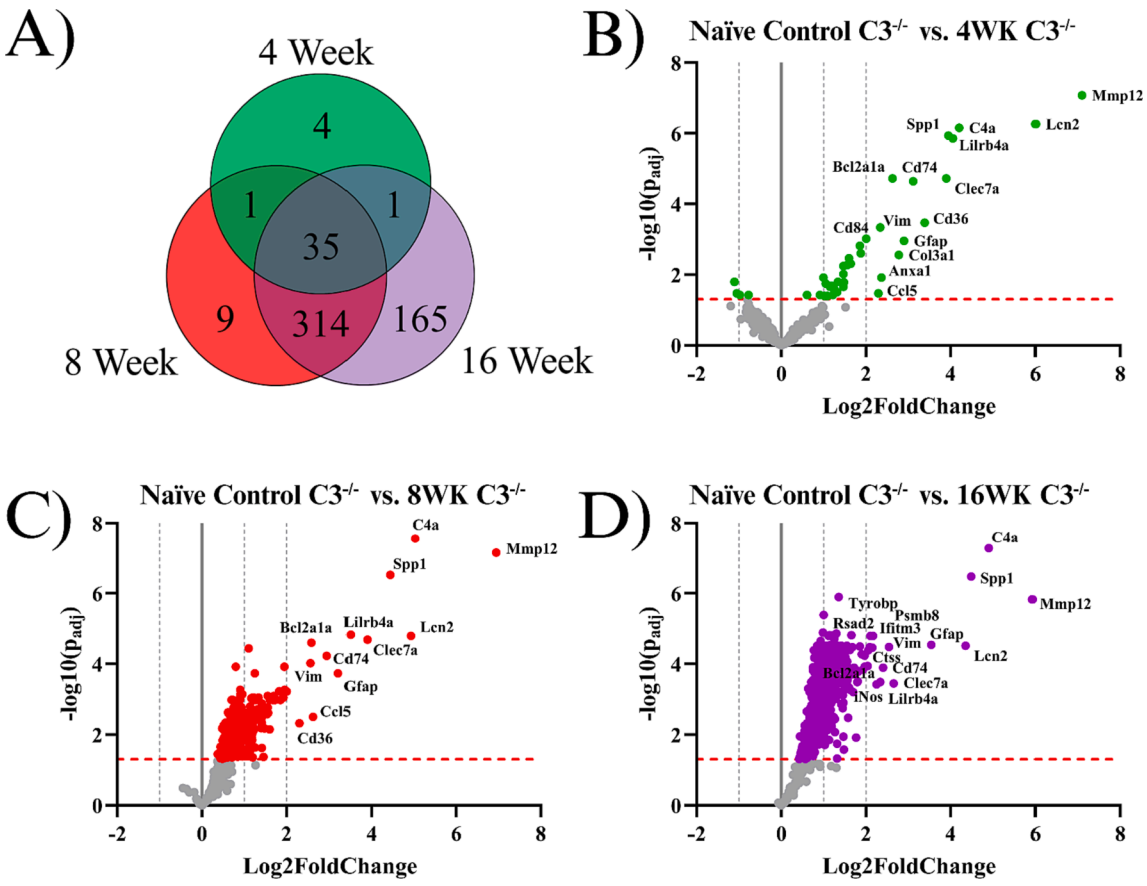

Fig. 1. Differential expression of neuroinflammatory genes in *C3*$^{-/-}$ post-surgery compared to *C3*$^{-/-}$ naïve control mice: A) Venn diagram indicating the number of differentially expressed genes. Gene expression levels for *C3*$^{-/-}$ mice surgically implanted with dummy probes were compared to *C3*$^{-/-}$ naïve control for each of the three time points we examined. Genes were included in the Venn diagram if $p_{adj} < 0.05$. Overlapping spaces in the diagram indicate the same genes demonstrating differential expression across multiple time points. The Venn diagram does not differentiate between up or down regulation. B-D) Volcano plots of all measured genes. All grey points represent insignificant genes and colored points represent genes found to be significant ($p_{adj} < 0.05$). The dashed red line represents the significance threshold and the dashed grey lines mark Log2FoldChange 1, −1, and 2 for reference. Due to space constraints, not all significant genes are labeled on the plots. Only genes with a Log2FoldChange > 1 or < -1 are labeled. For a complete list of differentially expressed genes, refer to Table 2 below. Each time point is plotted on a separate volcano plot. B) 4WK, C) 8WK, D) 16WK. (For interpretation of the references to colour in this figure legend, the reader is referred to the web version of this article.)

pathways had some significant genes at the 8WK time point, but to a much lesser extent. The majority of new differentially expressed genes are involved in pathways that were initiated in the 8WK time point, rather than adding entirely new pathways.

A total of 35 genes were upregulated in all three measured time points (Fig. 1A, Table S1). Five of the 35 overlapping genes are involved in lymphocyte activation (*Cd74, Irf8, Ptprc, Tgfb1, Plcg2*) (GO:0002285). Nine universally upregulated genes are associated with immunoglobulin-mediated immunity (*C1qa, Fcgr2b, Fcgr3, Ptpn6, Cd74, Ptprc, Tgfb1, Tcirg1, Trem2*) (GO:0016064). Other listed genes are expressed by B- or T-cells (*Blnk, Cd84, Tyrobp*) (Li, 2022; Fu, 1998; Zheng, 2022); macrophages or microglia *(Cd68, Spp1,Irf8, Mmp12, Mpeg1*) (Bayly-Jones, 2020; Masuda, 2012; Wells, 2003; Yeo, 2019; De Schepper, 2023), and astrocytes (*Gfap, Vim*) (Wilhelmsson, 2019). Several common biological functions such as antigen processing and presentation (*Ifi30, Cd74, Ctss*) (GO:0019882), phagocytosis (*Ctss, Cd36, Fcgr2b, Clec7a*) (GO:0006909), and complement activation (*C1qa, C3ar1, C4a*) (GO:006956) were found to be upregulated in all three time points. Overall, genes upregulated in the 4WK, 8WK, and 16WK time points are associated with general immune activation, which persists into chronic time points.

Taken together, in *C3*$^{-/-}$ mice, gene expression results in Fig. 1 suggest there is a trend toward upregulation of more genes with each successive measurement: i.e., from 4WK to 8WK to 16WK post-surgery. At 4WK post-surgery, the volcano plot is relatively symmetrical, with many genes showing increased and decreased Log2FoldChange below statistical and scientific significance. At 8WK post-surgery, the volcano plot skews toward the right, and at 16WK post-surgery, the volcano plot skews further right, with all genes showing upregulation. However, this is mainly in genes that have lower differential expression (Log2FoldChange of 0–1). In genes showing a high degree of upregulation starting at 4WK post-surgery, including *Mmp12*, *Lcn2*, *C4a*, *Lilrb4a, Clec7a*, *Spp1*, *Cd74*, *Gfap*, *Vim*, and *Bcl2a1,* the expression level remains stable over the 4-16WK post-surgical period. The more stable differentially upregulated genes includes the genes in the extracellular matrix system: *Mmp12*, *Spp1*; complement system: *C4a*; neutrophil degranulation system: *Lcn2*; and astrocyte structural proteins: *Gfap* and *Vim*, and are the same set of genes that show stable upregulation in WT mice at chronic timepoint (Song, 2023). In contrast, WT mice typically used for immunohistochemical analysis of the neuroinflammatory response generally demonstrate a stabilization of the neuroinflammatory response to intracortical microelectrodes over time (Jorfi, 2015; Usoro, 2021). Additionally, our own investigation of WT mice using identical methods found nearly stable gene expression from 4WK to 16WK post-surgery (Song, 2023).

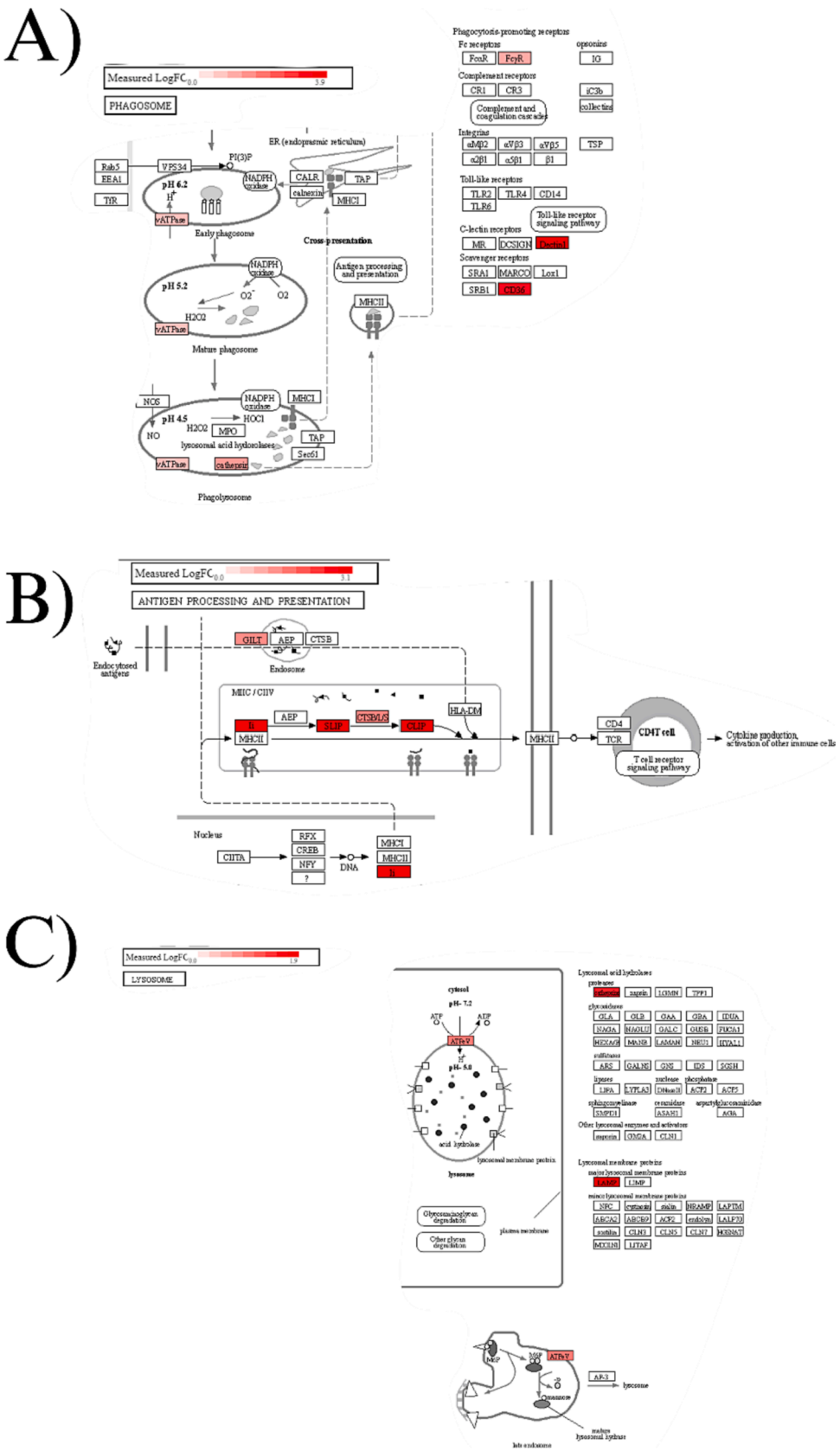

Fig. 2. Several key pathways upregulated in *C3*$^{-/-}$ 4WK mice compared to *C3*$^{-/-}$ naïve control mice. These figures were adapted from the full KEGG pathways, which are shown in Supplemental Fig. S3. A) Phagosome (KEGG:04145), B) Antigen processing and presentation (KEGG:04612), and C) Lysosome (KEGG:04142). Red indicates upregulation in the 4WK mice compared to naïve control, and blue indicates downregulation in 4WK mice compared to naïve control. No genes were downregulated in the 4WK mice. White indicates that the gene was not measured, or it showed no significant differential expression. (For interpretation of the references to colour in this figure legend, the reader is referred to the web version of this article.)

5. Neuroinflammatory gene expression to IME implantation in *C3*$^{-/-}$ vs WT mice

We also compared the expression of 826 genes in the neuroinflammatory pathway between *C3*$^{-/-}$ and WT, both in naïve control mice, and within 500 μm of the microelectrode-tissue interface mice at 4-, 8-, and 16-WK post-surgery. The naïve control *C3*$^{-/-}$ vs naïve control WT comparison informs us the state of the animal when they receive the implant, and the post-surgery time course comparisons illustrate how the temporal changes in neuroinflammation in mice lacking the C3 pathway, compared to WT mice.

Of the 826 genes measured, 423 were found to be differentially expressed between *C3*$^{-/-}$ and WT mice in at least 1 comparison. The remaining 403 genes were not differentially expressed between the two groups. Fig. 3A shows a Venn diagram of the gene expression profiles for each of the 4 comparisons. Overlapping regions illustrate differential expression in more than one comparison. Any gene found to be differentially expressed with $p_{adj} < 0.05$ was included.

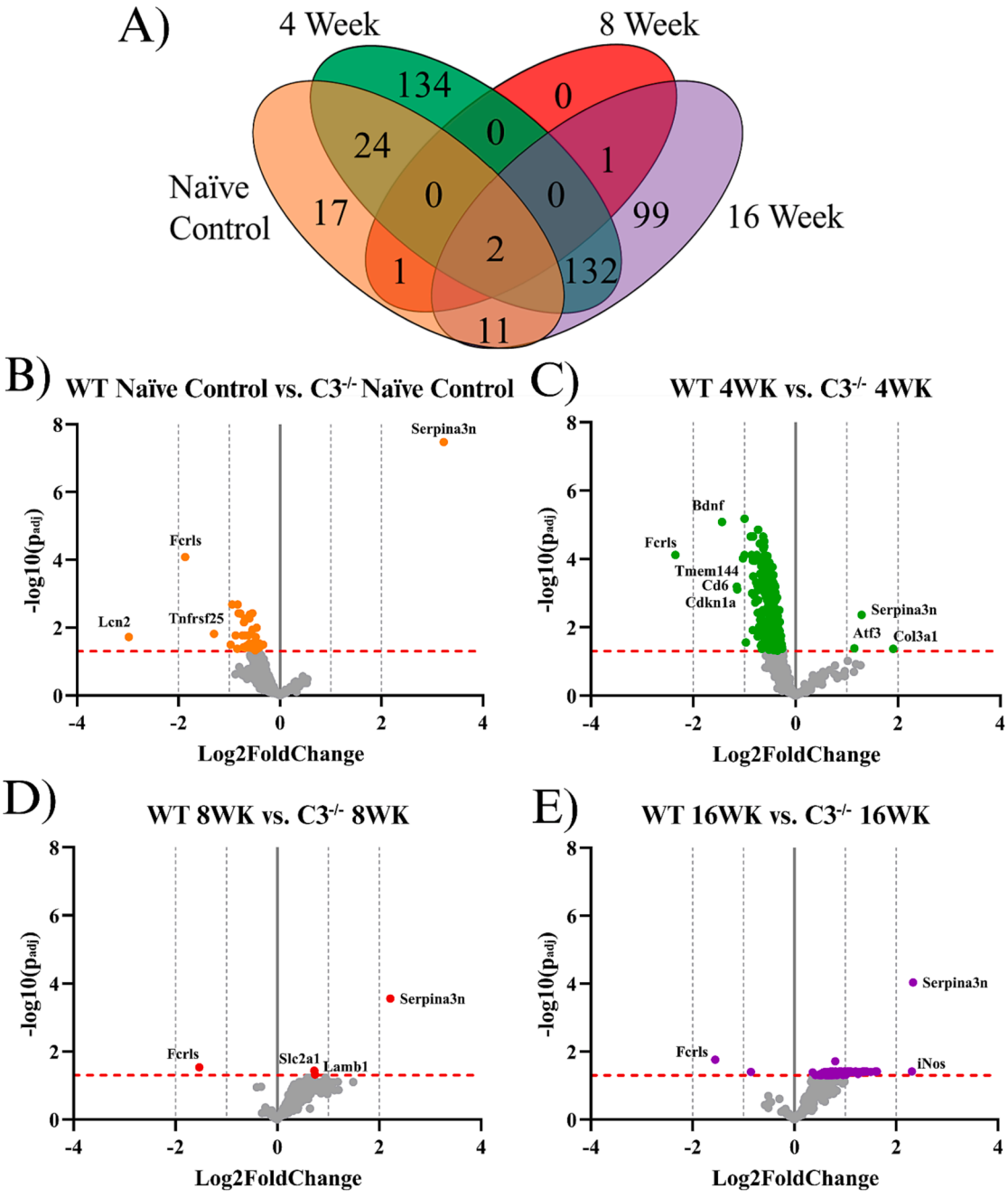

Fig. 3. Differential expression of neuroinflammatory genes *in C3*$^{-/-}$ post-surgery compared to WT mice: A) Venn diagram indicating the number of differentially expressed genes. Gene expression levels for *C3*$^{-/-}$ mice compared to WT mice for each of the four conditions we examined. Genes are included in the Venn diagram if $p_{adj} < 0.05$. Overlapping points on the diagram indicate the same genes demonstrating differential expression across multiple conditions. This figure does not differentiate between higher or lower expression. B-E) Volcano plots of all measured genes. All grey points represent insignificant genes and colored points represent genes found to be significant ($p_{adj} < 0.05$). The dashed red line represents the significance threshold and the dashed grey lines mark Log2FoldChange −2, −1, 1, and 2 for reference. Due to space constraints, not all significant genes are labeled. For a complete list of differentially expressed genes, refer to Table S2 below. Each condition is plotted on a separate volcano plot. B = naïve control, C = 4WK, D = 8WK, E = 16WK. (For interpretation of the references to colour in this figure legend, the reader is referred to the web version of this article.)

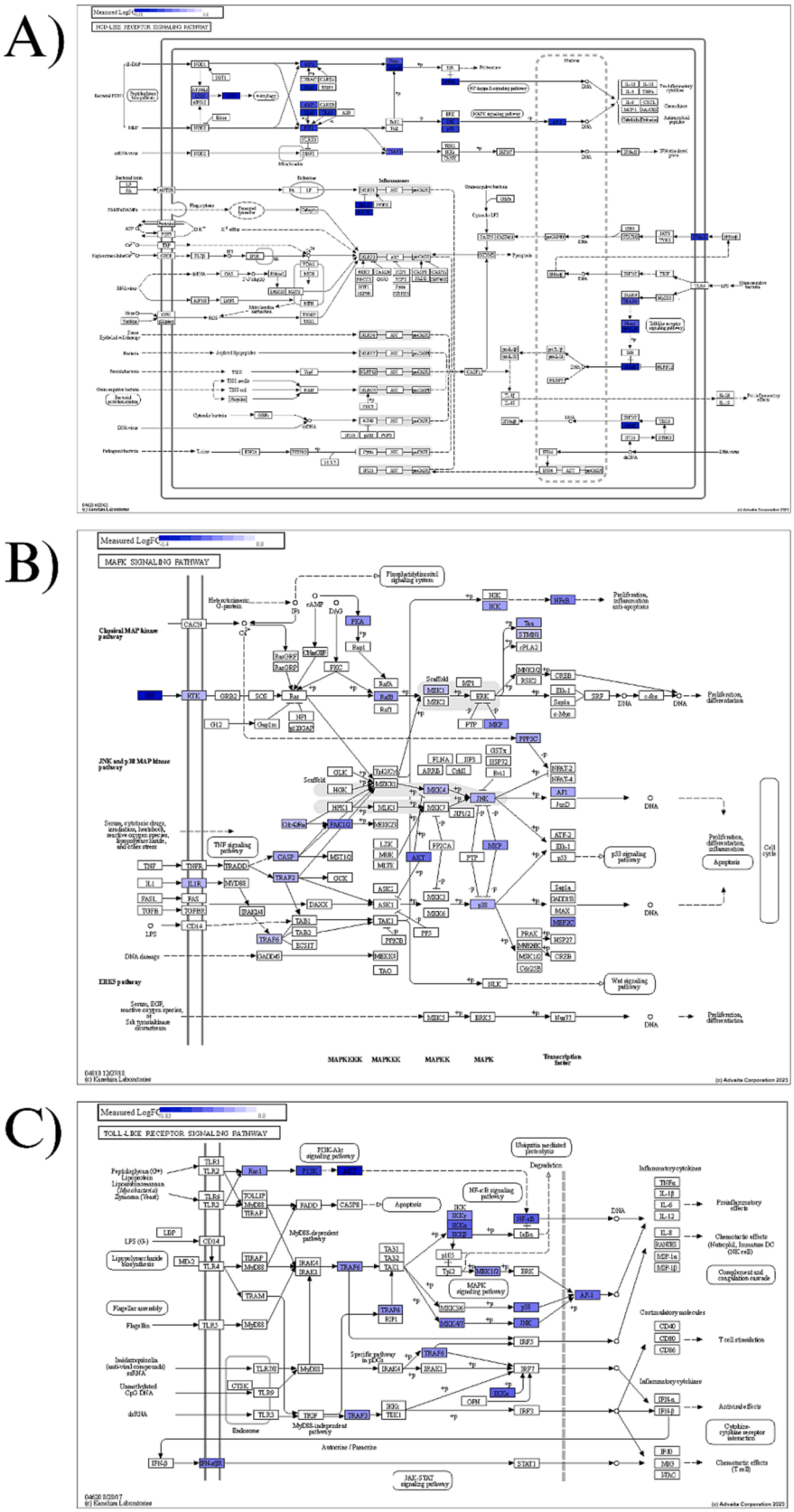

Fig. 4. Signaling pathways in *C3*$^{-/-}$ 4WK mice compared to WT 4WK mice that were also found in the *C3*$^{-/-}$ implanted mice compared to *C3*$^{-/-}$ naïve control comparison (Supplemental Fig. S4,3A.6). A) NOD-like receptor signaling (KEGG:04621), B) MAPK signaling (KEGG:04010), C) toll-like receptor signaling (KEGG:04620). Red indicates higher expression in the *C3*$^{-/-}$ mice compared to WT, and blue indicates lower expression in *C3*$^{-/-}$ mice compared to WT. No genes showed higher expression in the *C3*$^{-/-}$ mice. White indicates that the gene was not measured, or it showed no significant differential expression. (For interpretation of the references to colour in this figure legend, the reader is referred to the web version of this article.)

In naïve control animals, *C3*$^{-/-}$ mice showed overall decreased expression of neuroinflammatory genes compared to WT mice (Fig. 3A, 4B, Table S2). In naïve control mice, 56 genes showed statistically significant lower expression, and only one gene showed significantly higher expression in *C3*$^{-/-}$ mice, *Serpina3n* (Fig. 3B, Table S2). Four of these genes exhibit Log2FoldChange > 1 or < -1 (greater than 2-fold change in either direction): *Serpina3n*, *Lcn2*, *Fcrls*, and *Tnfrsf25*. These four genes are all known markers of neuroinflammation in some form. *Serpina3n* codes for the protein serine peptidase inhibitor clade A member 3n (SERPINA3N), it has been shown to inhibit the proteolytic activity of Cathepsin G, leukocyte elastase, granzymeB, and matrix metalloprotease 9 (Grafals and Thurman, 2019). *Serpina3n* is often expressed in neurons and astrocytes after injury (Mathern and Heeger, 2015). *Serpina3n* has been found to be both neuroprotective and neuroinflammatory (Liu, 2023). *Fcrls* codes for Fc Receptor Like S and is considered a microglial marker (Ravikumar, 2014), although one study has suggested that during chronic CNS injury, infiltrating macrophages may also express microglial markers, such as *Fcrls* (Grassivaro, 2020). *Lcn2,* another gene upregulated in the WT naïve control animals, codes for the protein lipocalin-2. In the brain, *Lcn2* is expressed by neurons and glial cells, and its expression can injure neurons directly and increase BBB permeability (Zhang, 2022). *Tnfrsf25*; which encodes for tumor necrosis factor receptor superfamily member 25, is also known as death domain receptor 3 (DR3). *Tnfrsf25* initiates apoptotic pathways in neurons and is required for the maintenance of the brain with age (Twohig and M.I.R., Nuria Gavalda, Emma L. Rees-Taylor, Albert Giralt, Debbie Adams, Simon P. Brooks, Melanie J. Bull, Claudia J. Calder, Simone Cuff, Audrey A. Yong, Jordi Alberch, Alun Davies, Stephen B. Dunnett, Aviva M. Tolkovsky, and Eddie C. Y. Wang, 2010). However, overexpression of *Tnfrsf25* could lead to excessive neuronal death. Additionally, six genes with lower expression: *Atm, Casp9, Trp53, Cdkn1a, Gadd45g, and Bcl2* are involved in the p53 signaling pathway. The p53 signaling pathway is activated by unhealthy cellular conditions such as oxidative stress and DNA damage and leads to apoptosis, dysfunction in cell proliferation, and stalled cellular growth (Supplemental Fig. S8A). The p53 signaling pathway seems to suggest that *C3*$^{-/-}$ naïve control mice are less susceptible to DNA damage and apoptosis, shown by higher *Atm* and *Casp9* expression, but have potentially lower chances of cell cycle arrest, shown by higher *Cdkn1a* and *Gadd45g* expression.

At 4WK post-surgery, *C3*$^{-/-}$ mice retained overall lower expression of neuroinflammatory genes compared to WT mice, with 300 genes showing lower expression and 3 genes showing higher expression (Fig. 3A, 3C and Table S2). Five genes showed statistically significant lower expression with Log2FoldChange < -1: *Bdnf*, *Fcrls*, *Tmem114*, *Cdkn1a*, and *Cd6,* and three genes showed significant higher expression with Log2FoldChange > -1: *Serpina3n*, *Arf3*, and *Col3a* in *C3*$^{-/-}$ mice compared to WT mice (Fig. 3C, Table S2). All of the neuroinflammary signaling (NOD-like receptor, MAPK, toll-like receptor, p53) and degenerative (apoptosis, neurodegeneration) pathways that were previously discussed in the 8WK and 16WK *C3*$^{-/-}$ vs naïve control *C3*$^{-/-}$ comparisons (Supplemental Figs. S2, S3, S5, S6) are also differentially expressed between *C3*$^{-/-}$ vs WT mice at 4WK (Fig. 3C, 4, 5); suggesting that the pathways that are damaging to the *C3*$^{-/-}$ animals at chronic time points are affecting WT mice at acute time points. Of the genes showing lower expression in *C3*$^{-/-}$ mice at 4WK, we now see differential expression of 13 genes associated with p53 signaling (Supplemental Fig. S8B), compared to 6 in the naïve control comparison (Supplemental Fig. S8A). From non-implanted animals to 4WK post sugery, the genes modulated by *Trp53* show more downregulation in the *C3*$^{-/-}$ animals. This means that *C3*$^{-/-}$ animals have lower initial expression of markers for damage and apoptosis compared to WT. Specifically, we now see lower expression of *Atr* in 4WK *C3*$^{-/-}$, which is a marker for DNA damage, and *Bid*, which signals for mitochondrial breakdown (Fig. 3C, Table S2, Supplemental Fig. S8B). *Trp53* (*p53*) itself, which is at the center of the p53 pathway, is no longer differentially expressed, despite the fact that genes *Trp53* acts on are differentially expressed (Fig. 3C, Table S2, Supplemental Fig. S8B). The other neuroinflammatory pathways previously discussed in the *C3*$^{-/-}$ implanted vs *C3*$^{-/-}$ naïve control comparison also have significant differential expression in the 4WK *C3*$^{-/-}$ vs 4WK WT comparison, with 18 NOD-like receptor pathway genes (Fig. 4A), 31 MAPK signaling pathway genes (Fig. 4B), and 19 toll-like receptor pathway genes (Fig. 4C) showing lower expression in the 4WK *C3*$^{-/-}$ animals (Fig. 3C, Table S2) compared to 4WK WT. 4WK *C3*$^{-/-}$ mice, in turn, displayed the higher expression of genes associated with apoptosis (31 genes, Fig. 3C, 5A, Table S2), autophagy (29 genes, Fig. 3C,5B, Table S2), and neurodegeneration (43 genes, Fig. 3C,5C Table S2). Combined, our results indicate that *C3*$^{-/-}$ mice are experiencing less severe neuroinflammation and degeneration at the 4WK acute time point. However, the acute response in *C3*$^{-/-}$ mice may also indicate that the removal of *C3* delays the neuroinflammatory response to IMEs, as the 8WK and 16WK results suggest.

At 8WK post-surgery, the trend of neuroinflammatory gene expression flips from showing higher differential expression in the WT mice to showing higher differential expression in the C3$^{-/-}$ mice. There were four genes showing significant differential expression: one showing higher expression, *Frcls*, and three showing lower expression, *Lamb1*, *Slc2a1*, and *Serpina3n*. (Fig. 3A, 3D, Table S2). Function of *Frcls* and *Serpina3n* have been described in previous sections. *Lamb1* codes for laminin subunit beta 1, an intermediate filament protein part of the nuclear envelope. Duplicates of the human ortholog of the *Lamb1* gene result in adult-onset autosomal-dominant leukodystrophy, a progressive fatal neurological disease (Burke and Stewart, 2014). *Slc2al* codes for solute carrier family 2/glucose transporter protein type 1 (*GLUT1*), which transports glucose across the blood–brain barrier and between glial cells (Devraj, 2011). In comparing *C3*$^{-/-}$ 8WK vs *C3*$^{-/-}$ naïve control, we found the 8WK to be the timepoint when many inflammatory signaling pathways are activated in the implanted *C3*$^{-/-}$ mice (Table S1, Fig. 1C, 3). Since 4WK shows significant downregulation of neuroinflammatory genes in *C3*$^{-/-}$, whereas 16WK shows significant upregulation, we consider 8WK to be the turning point, where few genes are differentially expressed because the *C3*$^{-/-}$ mice are no longer benefitting from the knockout, and inflammation is beginning to ramp up.

At 16WK post-surgery, *C3*$^{-/-}$ mice showed overall higher expression of neuroinflammatory genes compared to WT mice (Table S2, Fig. 3E). A total of 247 genes showed statistically significant differential expression, of which 2 showed lower expression and 245 showed higher expression in *C3*$^{-/-}$ mice. Of these genes, one gene, *Fcrls*, showed lower expression with Log2FoldChange < -1. *Fcrls* has shown lower expression in all *C3*$^{-/-}$ mice compared to WT, regardless of the time point. *Fcrls* is the most highly expressed gene in murine microglia, and though its function is not entirely known, lower expression of this gene could suggest lower microglial concentration or decreased functionality and activation (Butovsky, 2014), or it could suggest that *C3*$^{-/-}$ microglial cells have a different protein composition and express the gene less. There were 49 genes that showed higher expression with Log2FoldChange > 1 (Table S2, Fig. 3E). Of the genes that showed higher expression, 132 are shared with the 4WK *C3*$^{-/-}$ vs 4WK WT comparison, but instead of showing higher expression like at 4WK, they are now showing lower expression at 16WK. This indicates that the same genes that were improving the response in the 4WK *C3*$^{-/-}$ mice are now contributing to the more robust inflammation at the 16WK time point. These 132 genes were not identified as clearly being part of specific signaling pathways but are associated with neuronal remodeling (GO:0030030), ATP hydrolysis (GO:0016887), and nucleotide binding (GO:0000166). Nucleotide binding and ATP hydrolysis are likely being activated due to high levels of transcription and translation as well as energy consumption from cell remodeling and healing.

As previously stated in the 16WK *C3*$^{-/-}$ vs naïve control comparison, 16WK *C3*$^{-/-}$ mice express several key pathways related to neural cell adhesion and remodeling. Those pathways are not found to be as activated in WT mice. In the axon guidance pathway (Fig. 6A), 9 genes are

differentially upregulated in the 16WK $C3^{-/-}$ mice vs WT. Ras signaling has 22 upregulated genes (Fig. 6B), Rap1 signaling has 17 upregulated genes (Figure 8C), and ErbB signaling has 12 upregulated genes (Figure 8D). There is also upregulation of the following pathways: NOD-like receptor signaling (14 genes; Supplemental Fig. S9A), MAPK signaling (26 genes; Supplemental Fig. S9B), toll-like receptor signaling (13 genes; Supplemental Fig. S9C), and p53 signaling (7 genes; Supplemental Fig. S9D). This means that the 16WK $C3^{-/-}$ mice show upregulation for neuroinflammation and signaling pathways that result in apoptosis and neuronal death, but also show many differentially expressed genes associated with remodeling.

Overall, we see that compared to WT animals, $C3^{-/-}$ mice demonstrate less inflammatory activity both before surgery and at 4WK post-surgery. At 8WK post-surgery, we see that $C3^{-/-}$ and WT animals exhibit very similar gene expression profiles. Finally, when we compare 16WK $C3^{-/-}$ mice to 16WK WT mice, we see that the $C3^{-/-}$ mice present with a more robust neuroinflammatory response. In WT mice, gene expression analysis has shown relatively stable responses over chronic time points (Song, 2023), but in the $C3^{-/-}$ mice there are pathways that suggest that the wound is still healing and the neural cells are still adapting to the implant. In all $C3^{-/-}$ vs WT comparisons, only 2 genes showed consistent differential expression. *Serpina3n* consistently showed higher expression in the $C3^{-/-}$ mice, and *Fcrls* consistently showed lower expression in $C3^{-/-}$ mice.

6. Discussion

In this study, we investigated the role of *C3* in the IME inflammatory response by comparing the neuroinflammatory gene expression at the microelectrode implant site between *C3* knockout ($C3^{-/-}$) and wild-type (WT) mice. We first investigated the changes in gene expression of $C3^{-/-}$ mice implanted with microelectrodes by comparing each post-surgical timepoint to naïve control. We found that in $C3^{-/-}$ mice, there are progressively more genes in the neuroinflammatory pathway showing upregulation from 4WK to 16WK post-surgery compared to naïve control (Fig. 1). Overall, these trends show that $C3^{-/-}$ leads to an initial reduction in neuroinflammatory process that transitions around 8WK post-surgery to an increase in neuroinflammatory process. Signaling pathways such as NOD-like, toll-like receptors, MAPK, and p53 show upregulation beginning at 8WK post-surgery (Fig. 1, Supplemental Fig. S2). Because of this, we believe that *C3* may be a potential therapeutic target acutely after microelectrode implantation. However, our results suggest that *C3* should not be targeted into chronic time points. Future studies could illuminate and optimize *C3*-targeting therapeutic schedule.

The genes stably showing upregulation after implantation – *Mmp12*, *Lcn2*, *C4a*, *Lilrb4a*, *Clec7a*, *Spp1*, *Cd74*, *Gfap*, *Vim*, and *Bcl2a1* – may serve as independent therapeutic targets (Fig. 1). These genes demonstrate stable upregulation in both WT and in $C3^{-/-}$ mice, which indicates that they are important tissue response genes at chronic time points in both genotypes of mice. These ten genes can be targeted independently of *C3* inhibition, with *C3* inhibition for a synergistic effect, or targeted after an initial 4 week-long course of *C3* inhibition.

When comparing the neuroinflammatory response in $C3^{-/-}$ mice to WT mice (Fig. 3), we found that there is an initial lower expression in neuroinflammatory genes in naïve $C3^{-/-}$ mice and during 4WK post-surgery timepoint. $C3^{-/-}$ naïve control mice showed lower expression in several inflammatory genes compared to WT naïve control mice, which suggests that $C3^{-/-}$ mice could be in a more favorable state to receive the implant (Fig. 3B, C). Therapeutically, such results would suggest treating participants with anti-C3 therapies prior to implantation could improve initial device performance. Once the implant is inserted, we see at the 4WK time point that NOD-like receptor, toll-like receptor, MAPK, and p53 signaling pathways are downregulated in $C3^{-/-}$ mice (Fig. 5). These pathways, along with many other genes downregulated in the $C3^{-/-}$ group, have pro-inflammatory and cytotoxic effects that the $C3^{-/-}$ mice are able to avoid. At 8WK post-surgery, we see the trend in differential gene expression start to shift towards $C3^{-/-}$ mice

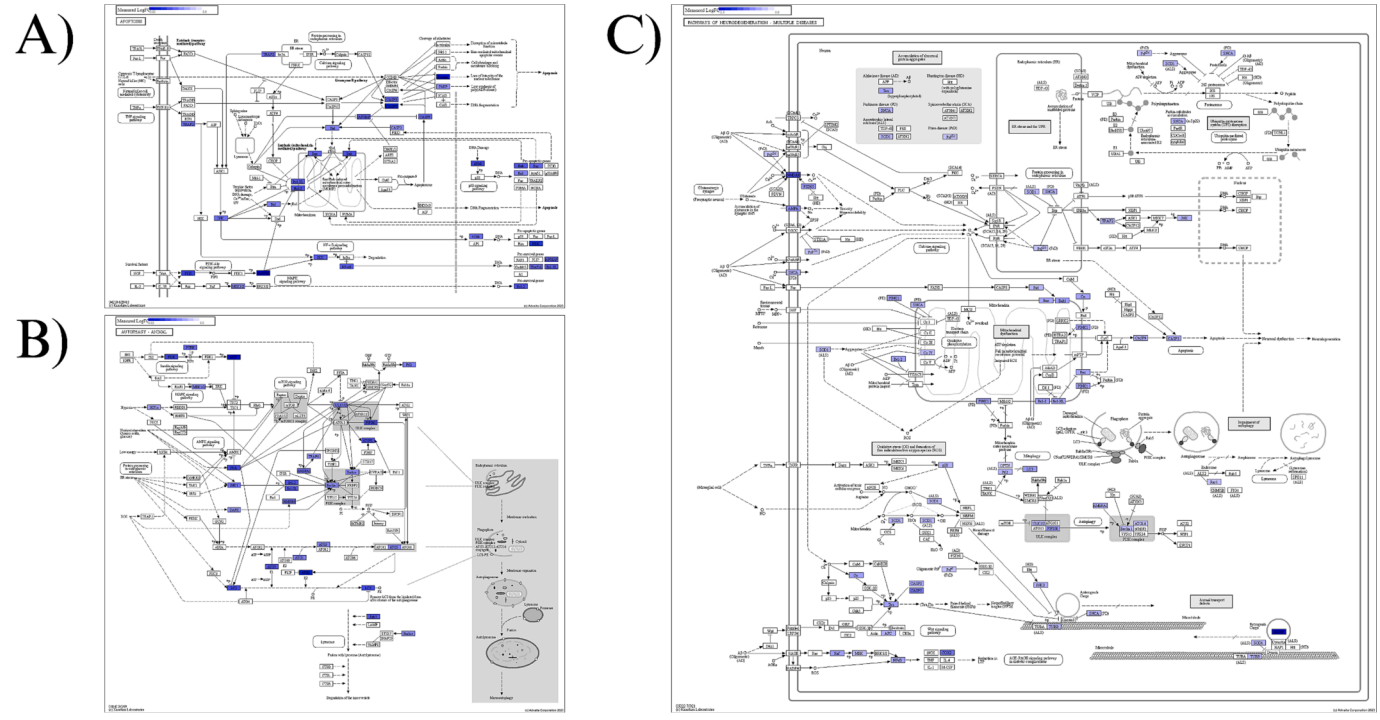

Fig. 5. Cell damage and death-related pathways in $C3^{-/-}$ 4WK mice compared to WT 4WK mice. A) apoptosis (KEGG:04210), B) autophagy (KEGG:04140), C) neurodegeneration (KEGG:05022). Red indicates higher expression in the $C3^{-/-}$ mice compared to WT, and blue indicates lower expression in $C3^{-/-}$ mice compared to WT. No genes showed higher expression in the $C3^{-/-}$ mice. White indicates that the gene was not measured, or it showed no significant differential expression. (For interpretation of the references to colour in this figure legend, the reader is referred to the web version of this article.)

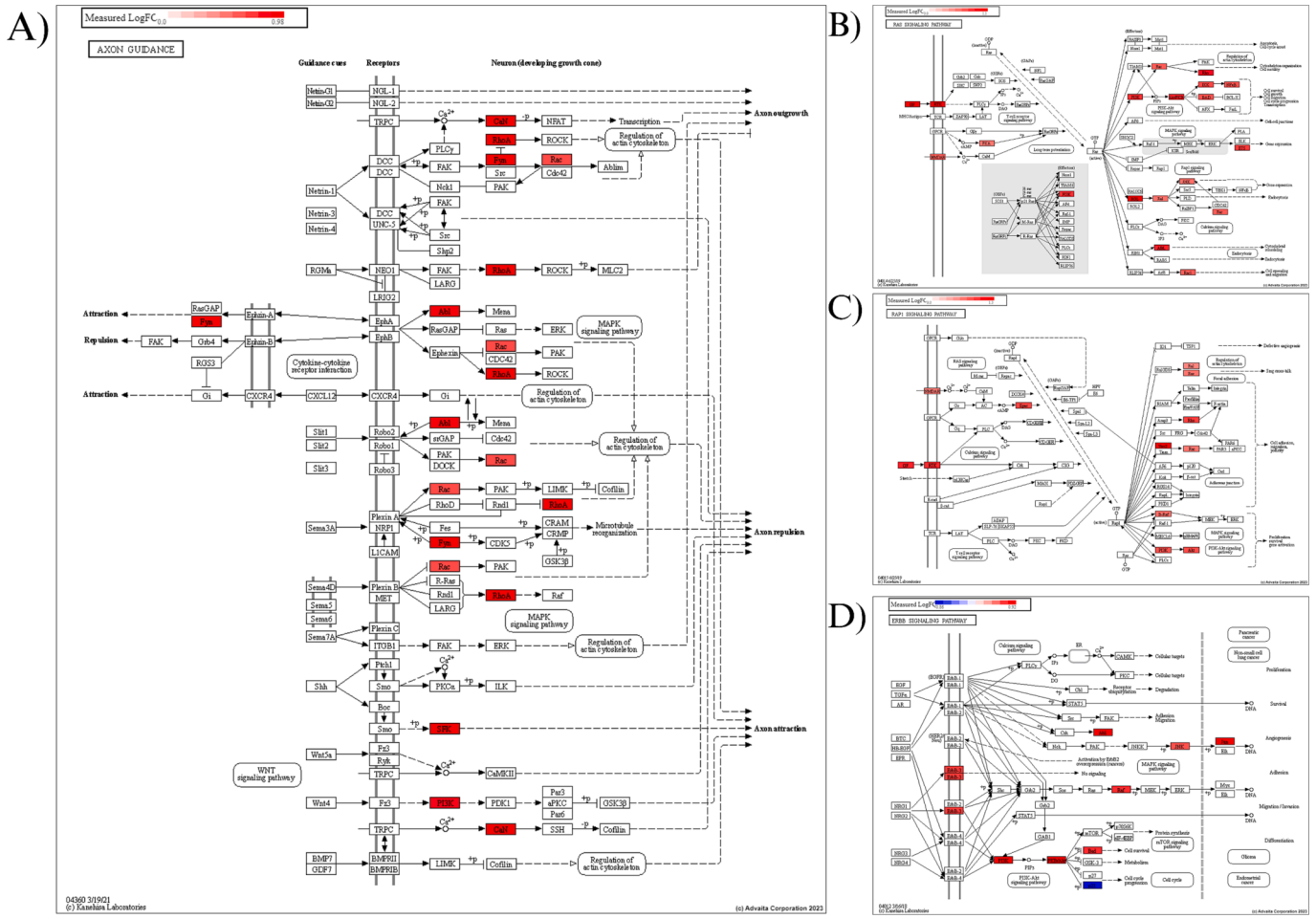

Fig. 6. Pathways in *C3*$^{-/-}$ 16WK mice compared to WT 16WK mice. A) axon guidance (KEGG:04360), B) Ras signaling (KEGG:04014), C) Rap1 signaling (KEGG:04015), and D) ErbB signaling (KEGG:04012). These can be compared to the same pathways found to be differentially expressed in the *C3*$^{-/-}$ 16WK mice compared to *C3*$^{-/-}$ naïve control comparison. Red indicates higher expression in the *C3*$^{-/-}$ mice compared to WT, and blue indicates lower expression in *C3*$^{-/-}$ mice compared to WT. White indicates that the gene was not measured or it showed no significant differential expression. (For interpretation of the references to colour in this figure legend, the reader is referred to the web version of this article.)

experiencing increased inflammation, with the gene expression profile being very similar to the WT mice (Fig. 3D). Finally, by 16WK, the *C3*$^{-/-}$ mice show increased differential neuroinflammatory gene expression compared to WT mice (Fig. 3E). Our findings suggest that knocking out *C3* essentially delays major components of the neuroinflammatory response, likely due to the absence of *C3* in the initiation of the foreign body response. The high differential expression of NOD-like receptor, toll-like receptor, MAPK, and p53 signaling pathways (Supplemental Figs. S8, S9) in *C3*$^{-/-}$ mice may point to them as potential targets alongside *C3*. Specifically, the toll-like receptor pathway is known to activate NOD-like and MAPK signaling, and targeting the toll-like receptor pathway has shown some success in IME applications (Bedell, 2020).

Additionally, at 16WK was when the *C3*$^{-/-}$ mice expressed many pathways associated with cell migration, extension, and adhesion (Fig. 6, Supplemental Fig. S7). The expression of these pathways suggests that in *C3*$^{-/-}$ mice, neural cells are still shifting around the implant site. This could be a result of the delayed neuroinflammatory response shown up to the 4WK time point, and it would be interesting to see if this effect lasts longer than 16WK post-surgery.

The only two genes showing consistent differences in expression between *C3*$^{-/-}$ and WT mice were *Serpina3n* and *Fcrls*. *Fcrls* shows consistently lower expression in the *C3*$^{-/-}$ and likely contributes to the inflammatory response, however the gene does not have a known human ortholog and therefore may not be relevant to clinical translation of implanted neural interfacing devices. *Serpina3n* encodes for the protein serine peptidase inhibitor clade A member 3n (SERPINA3N), and it is orthologous to a1-antichymotrypsin in humans. *Serpina3n* has been shown to inhibit the proteolytic activity of Cathepsin G, leukocyte elastase, granzyme B, and matrix metalloprotease 9 (Wang, 2020). It is often expressed in neurons and astrocytes after injury (Zamanian, 2012), and has been found overexpressed in mouse models of Alzheimer's disease and prion disease (Zattoni, 2022). There are conflicting reports of the role of *Serpina3n* in neuroinflammation. Multiple studies have found it to be neuroprotective: higher *Serpina3n* expression is associated with attenuating neuropathic pain, reducing severity of Multiple Sclerosis, and reducing tissue damage in ischemic stroke (Zhang, 2022). Thus, higher expression of *Serpina3n* in *C3*$^{-/-}$ mice compared to WT mice may be neuroprotective post-surgery. However, in one study of mice treated with neurotoxin; the neuro-protective effect of treatment was lost when associated with *Serpina3n* overexpression (Xi, 2019), and another found it to be pro-inflammatory in epileptic mice (Liu, 2023). A mechanistic understanding of *Serpina3n* may resolve these conflicting results. We have not yet found any direct studying linking the activity of protein SERPINA3n and complement factors, and it would be interesting to study the mechanism through which *C3* regulates *Serpina3n* expression, and how the protein products interact with each other. Because *Serpina3n* shows consistent higher expression in *C3*$^{-/-}$ mice compared to WT mice, although we do not know the exact interaction between *C3* and *Serpina3n*, *Serpina3n* expression could represent an alternative

pathway that leads to the increase in neuroinflammation in *C3*$^{-/-}$ mice at 8WK–16WK post-surgery and could be explored as a potential co-therapeutic target.

7. Conclusion

In this study, we investigated the effects of *C3* depletion on the neuroinflammatory process at the tissue-microelectrode interface by 1) investigating the changes in neuroinflammatory gene expression of *C3*$^{-/-}$ mice at 4—8-, and 16WK post-surgery compared to naïve control *C3*$^{-/-}$ mice, and 2) investigating neuroinflammatory gene expression of *C3*$^{-/-}$ mice at each pre- and post-surgical time point compared to time point-matched WT mice.

We found that in *C3*$^{-/-}$ mice there is at lower expression of neuroinflammatory genes prior to implantation, and at 4WK post-surgery compared to WT mice. There is a trend towards increasing expression of neuroinflammatory genes between 8 and 16WK post-surgery in *C3*$^{-/-}$ mice, and by 16WK post-surgery there is an increase in expression of neuroinflammatory genes compared to WT control. While neuroinflammatory gene expression profiles suggest that *C3* is a potential early therapeutic target for reducing neuroinflammation at the tissue-microelectrode interface, the duration, timing, and frequency of the therapy cycle must be investigated and optimized in future studies.

Currently, gene therapy to mediate complement system activity has not been clinically approved. Genetic silencing of C5 has undergone phase 1 and 2 clinical trials, but no results from these studies have been published to date (https://clinicaltrials.gov/ct2/show/NCT03303313) (Garred et al., 2021). However, other methods of preventing full complement activation have been developed. Compstatin is a peptide that binds to C3 and blocks C3 cleavage and subsequent complement activation, and has been FDA approved in the form of pegcetacoplan (Empaveli) (Mastellos, 2022). Eculizumab (Soliris™) is a C5 blocking antibody that is used to mediate complement-driven inflammation (Dmytrijuk, 2008). Targeting the complement system can be difficult due to both high concentration of complement proteins throughout the body and the body's quick response to changes in complement expression (Dreismann, 2023). Delivery methods would also need to be very precise to preserve healthy complement activation in uninjured/inflamed regions.

Genes showing high upregulation: *Mmp12*, *Lcn2*, *C4a*, *Lilrb4a*, *Clec7a*, *Spp1*, *Cd74*, *Gfap*, *Vim*, and *Bcl2a1* show stable and consistent higher expression over the course of this study in *C3*$^{-/-}$ mice and in WT mice (Bedell, 2020; Song, 2023; Song and H.W.B., B.J. Regan, E.S. Ereifej, R. Chan, J.R. Capadona, 2022). There genes may represent underlying chronic neuroinflammatory response to microelectrodes and could be investigated as independent therapeutic targets, either alone or in combination with *C3* inhibition to reduce inflammatory process at tissue-microelectrode interface. *Serpina3n* and *Fcrls* shows consistent higher and lower expression, respectively, in *C3*$^{-/-}$ mice compared to timepoint matched WT mice and could be a pathway through which *C3* regulations neuroinflammation. Increase in *Serpina3n* expression, especially, could represent compensatory pathways through which *C3* depletion eventually leads to an increase in neuroinflammatory gene expression, and should be investigated as a potential co-therapeutic target. Genes such as *Serpina3n, Mmp12*, *Lcn2*, *C4a*, *Lilrb4a*, *Clec7a*, *Spp1*, *Cd74*, *Gfap*, *Vim*, and *Bcl2a1* that have been identified in this study as potential targets for IME improvement could also be applied to other related fields, such as deep brain stimulating electrode implantation and general traumatic brain injury.

One limitation of our study is that we looked only at time points weeks after implantation. Because in *C3*$^{-/-}$ mice there is a change in expression level over the course of 4 – 16WK post-surgery, we cannot extrapolate what the expression level may look like at acute timepoints of hours to 4WK post-surgery, where gene expression is even more dynamic. Future studies should investigate neuroinflammatory expression in *C3*$^{-/-}$ mice at acute timepoints and compare to WT mice. Another limitation is the lack of spatial resolution. Gene expression at tissue-microelectrodes can vary greatly even at the micron scale, and higher spatial resolution would be more informative on the changes in gene expression closer to tissue microelectrode interface. A final limitation of our study is that we did not investigate the expression and activity of proteins. Although gene expression studies can help inform us on the cellular processes behind the neuroinflammatory response to microelectrodes, ultimately, protein function drives cellular processes. Future works should study the correlation between gene expression and protein expression, modification, and activity.

This study was supported in part by Merit Review Award GRANT12418820 (Capadona) and Senior Research Career Scientist Award # GRANT12635707 (Capadona) from the United States (US) Department of Veterans Affairs Rehabilitation Research and Development Service. Additionally, this work was also supported in part by the National Institute of Health, National Institute of Neurological Disorders and Stroke GRANT12635723 (Capadona/Pancrazio), and the National Institute for Biomedical Imaging and Bioengineering, T32EB004314, (Capadona/Kirsch). Finally, this work is supported by the National Institute of Health, National Institute for General Medical Sciences Institutional National Research Service Award T32GM007250 and National Institute of Health, Clinical and Translational Science Award TL1TR000441.

CRediT authorship contribution statement

Sydney S. Song: Conceptualization, Data curation, Formal analysis, Investigation, Methodology, Writing – review & editing. **Lindsey N. Druschel:** Data curation, Formal analysis, Investigation, Methodology, Supervision, Validation, Visualization, Writing – original draft. **Jacob H. Conard:** Investigation, Writing – review & editing. **Jaime J. Wang:** Investigation, Methodology, Validation, Writing – review & editing. **Niveda M. Kasthuri:** Data curation, Investigation, Validation, Writing – review & editing. **E. Ricky Chan:** Validation. **Jeffrey R. Capadona:** Conceptualization, Funding acquisition, Project administration, Resources, Supervision, Writing – review & editing.

Declaration of competing interest

The authors declare that they have no known competing financial interests or personal relationships that could have appeared to influence the work reported in this paper.

Data availability

Data will be made available on request.

Appendix A. Supplementary data

Supplementary data to this article can be found online at https://doi.org/10.1016/j.bbi.2024.03.004.

References

Ajiboye, A.B., et al., 2017. Restoration of reaching and grasping movements through brain-controlled muscle stimulation in a person with tetraplegia: a proof-of-concept demonstration. Lancet 389 (10081), 1821–1830.
Ashburner, M., et al., 2000. Gene ontology: tool for the unification of biology. The Gene Ontology Consortium. Nat. Genet. 25 (1), 25–29.
Bayly-Jones, C., et al., 2020. Ancient but not forgotten: new insights into MPEG1, a macrophage perforin-like immune effector. Front. Immunol. 11, 581906.
Bedell, H.W., et al., 2018. Understanding the effects of both CD14-meditated innate immunity and device/tissue mechanical mismatch in the neuroinflammatory response to intracortical microelectrodes. Front. Neurosci. 12, 772.
Bedell, H.W., et al., 2020. Differential expression of genes involved in the acute innate immune response to intracortical microelectrodes. Acta Biomater. 102, 205–219.
Bennett, C., et al., 2021. The complement cascade at the Utah microelectrode-tissue interface. Biomaterials 268, 120583.

Bjornsson, C.S., et al., 2006. Effects of insertion conditions on tissue strain and vascular damage during neuroprosthetic device insertion. J. Neural Eng. 3 (3), 196–207.
Brommer, B., et al., 2016. Spinal cord injury-induced immune deficiency syndrome enhances infection susceptibility dependent on lesion level. Brain 139 (Pt 3), 692–707.
Buchman, A.L., 2001. Side effects of corticosteroid therapy. J. Clin. Gastroenterol. 33 (4), 289–294.
Burke, B., Stewart, C.L., 2014. Functional architecture of the cell's nucleus in development, aging, and disease. Curr. Top. Dev. Biol. 109, 1–52.
Butovsky, O., et al., 2014. Identification of a unique TGF-beta-dependent molecular and functional signature in microglia. Nat. Neurosci. 17 (1), 131–143.
Carpanini, S.M., Torvell, M., Morgan, B.P., 2019. Therapeutic inhibition of the complement system in diseases of the central nervous system. Front. Immunol. 10, 362.
Curran, J., et al., 2022. Estimating daily antibiotic harms: an umbrella review with individual study meta-analysis. Clin. Microbiol. Infect. 28 (4), 479–490.
Daei Sorkhabi, A., et al., 2023. The safety and efficacy of tislelizumab, alone or in combination with chemotherapy, for the treatment of non-small cell lung cancer: a systematic review of clinical trials. BMC Pulm. Med. 23 (1), 495.
De Schepper, S., et al., 2023. Perivascular cells induce microglial phagocytic states and synaptic engulfment via SPP1 in mouse models of alzheimer's disease. Nat. Neurosci. 26 (3), 406–415.
Devraj, K., et al., 2011. GLUT-1 glucose transporters in the blood-brain barrier: differential phosphorylation. J. Neurosci. Res. 89 (12), 1913–1925.
Dmytrijuk, A., et al., 2008. FDA report: eculizumab (soliris) for the treatment of patients with paroxysmal nocturnal hemoglobinuria. Oncologist 13 (9), 993–1000.
Donato, M., et al., 2013. Analysis and correction of crosstalk effects in pathway analysis. Genome Res. 23 (11), 1885–1893.
Draghici, S., et al., 2007. A systems biology approach for pathway level analysis. Genome Res. 17 (10), 1537–1545.
Dreismann, A.K., et al., 2023. Gene targeting as a therapeutic avenue in diseases mediated by the complement alternative pathway. Immunol. Rev. 313 (1), 402–419.
Ekdahl, K.N., et al., 2011. Innate immunity activation on biomaterial surfaces: a mechanistic model and coping strategies. Adv. Drug Deliv. Rev. 63 (12), 1042–1050.
Ereifej, E.S., et al., 2018. Implantation of neural probes in the brain elicits oxidative stress. Front. Bioeng. Biotechnol. 6, 9.
Ereifej, E.S., et al., 2018. The neuroinflammatory response to nanopatterning parallel grooves into the surface structure of intracortical microelectrodes. Adv. Funct. Mater. 28 (12), 1704420.
Falcone, J.D., et al., 2018. Correlation of mRNA expression and signal variability in chronic intracortical electrodes. Front. Bioeng. Biotechnol. 6, 26.
Fatima, N., Shuaib, A., Saqqur, M., 2020. Intra-cortical brain-machine interfaces for controlling upper-limb powered muscle and robotic systems in spinal cord injury. Clin. Neurol. Neurosurg. 196, 106069.
Fu, C., et al., 1998. BLNK: a central linker protein in B cell activation. Immunity 9 (1), 93–103.
Garred, P., Tenner, A.J., Mollnes, T.E., 2021. Therapeutic targeting of the complement system: from rare diseases to pandemics. Pharmacol. Rev. 73 (2), 792–827.
Gene Ontology, C., et al., 2023. The gene ontology knowledgebase in 2023. Genetics 224 (1).
Golabchi, A., et al., 2018. Melatonin improves quality and longevity of chronic neural recording. Biomaterials 180, 225–239.
Golabchi, A., et al., 2020. Neuroadhesive protein coating improves the chronic performance of neuroelectronics in mouse brain. Biosens. Bioelectron. 155, 112096.
Grafals, M., Thurman, J.M., 2019. The role of complement in organ transplantation. Front. Immunol. 10, 2380.
Grassivaro, F., et al., 2020. Convergence between microglia and peripheral macrophages phenotype during development and neuroinflammation. J. Neurosci. 40 (4), 784–795.
Haley, R.M., et al., 2020. Resveratrol delivery from implanted cyclodextrin polymers provides sustained antioxidant effect on implanted neural probes. Int. J. Mol. Sci. 21 (10).
Harris, J.P., et al., 2011. Mechanically adaptive intracortical implants improve the proximity of neuronal cell bodies. J. Neural Eng. 8 (6), 066011.
He, W., McConnell, G.C., Bellamkonda, R.V., 2006. Nanoscale laminin coating modulates cortical scarring response around implanted silicon microelectrode arrays. J. Neural Eng. 3 (4), 316–326.
Heelan, C., et al., 2019. Decoding speech from spike-based neural population recordings in secondary auditory cortex of non-human primates. Commun Biol 2 (1), 466.
Heianza, Y., et al., 2020. Duration and life-stage of antibiotic use and risks of all-cause and cause-specific mortality: prospective cohort study. Circ. Res. 126 (3), 364–373.
Hermann, J.K., et al., 2018. Inhibition of the cluster of differentiation 14 innate immunity pathway with IAXO-101 improves chronic microelectrode performance. J. Neural Eng. 15 (2), 025002.
Hernandez-Reynoso, A.G., et al., 2023. The effect of MnTBAP coatings on the acute and sub-chronic recording performance of planar silicon intracortical microelectrode arrays. Biomaterials. Accepted - In press.
Hochberg, L.R., et al., 2006. Neuronal ensemble control of prosthetic devices by a human with tetraplegia. Nature 442 (7099), 164–171.
Hochberg, L.R., Donoghue, J.P., 2006. Sensors for brain-computer interfaces. IEEE Eng. Med. Biol. Mag. 25 (5), 32–38.
Hoeferlin, G.F., Bajwa, T., Olivares, H., Zhang, J., Druschel, L.N., Sturgill, B., Sobota, M., Boucher, P., Duncan, J., Hernandez-Reynoso, A.G., Cogan, S.F., Pancrazio, J.J., Capadona, J.R., 2023. Antioxidant Dimethyl Fumarate Temporarily but not Chronically Improves Microelectrode Performance. Micromachines 14 (10), 1902.
Hubel, D.H., 1957. Tungsten microelectrode for recording from single units. Science 125 (3247), 549–550.
Hubel, D.H., Wiesel, T.N., 1959. Receptive fields of single neurones in the cat's striate cortex. J. Physiol. 148, 574–591.
Irwin, Z.T., et al., 2017. Neural control of finger movement via intracortical brain–machine interface. J. Neural Eng. 14 (6), 066004.
Jarosiewicz, B., et al., Virtual typing by people with tetraplegia using a self-calibrating intracortical brain-computer interface. Sci. Transl. Med., 2015. 7(313): p. 313ra179.
Jorfi, M., et al., 2015. Progress towards biocompatible intracortical microelectrodes for neural interfacing applications. J. Neural Eng. 12 (1), 011001.
Julia Minkiewicz, J.P.d.R.V., Robert W. Keane, Human astrocytes express a novel NLRP2 inflammasome. Glia, 2013. 61(7): p. 1113-1121.
Kaki, R., et al., 2011. Impact of antimicrobial stewardship in critical care: a systematic review. J. Antimicrob. Chemother. 66 (6), 1223–1230.
Kanehisa, M., 2019. Toward understanding the origin and evolution of cellular organisms. Protein Sci. 28 (11), 1947–1951.
Kanehisa, M., Goto, S., 2000. KEGG: Kyoto encyclopedia of genes and genomes. Nucleic Acids Res. 28 (1), 27–30.
Kanehisa, M., et al., KEGG for taxonomy-based analysis of pathways and genomes. Nucleic Acids Res, 2023. 51(D1): p. D587-D592.
Khorasani, A., et al., 2016. Continuous force decoding from local field potentials of the primary motor cortex in freely moving rats. Sci. Rep. 6 (1), 35238.
Kim, Y., et al., 2021. Ventricular delivery of resveratrol improves microelectrode recording performance and reduces oxidative stress. Micromachines 12, 1446.
Kozai, T.D., et al., 2014. Effects of caspase-1 knockout on chronic neural recording quality and longevity: insight into cellular and molecular mechanisms of the reactive tissue response. Biomaterials 35 (36), 9620–9634.
Kozai, T.D.Y., et al., 2015. Brain tissue responses to neural implants impact signal sensitivity and intervention strategies. ACS Chem. Nerosci. 6 (1), 48–67.
L., m.,, 2004. Cyclooxygenase-2 (COX-2) in inflammatory and degenerative brain diseases. J. Neuropathol. Exp. Neurol. 63 (9), 901–910.
Li, J., et al., KIR(+)CD8(+) T cells suppress pathogenic T cells and are active in autoimmune diseases and COVID-19. Science, 2022. 376(6590): p. eabi9591.
Liu, C., et al., 2023. Astrocyte-derived SerpinA3N promotes neuroinflammation and epileptic seizures by activating the NF-kappaB signaling pathway in mice with temporal lobe epilepsy. J. Neuroinflammation 20 (1), 161.
Liu, C., et al., 2023. Astrocyte-derived SerpinA3N promotes neuroinflammation and epileptic seizures by activating the NF-κB signaling pathway in mice with temporal lobe epilepsy. J. Neuroinflammation 20 (1), 161.
Lubbers, R., et al., 2017. Production of complement components by cells of the immune system. Clin. Exp. Immunol. 188 (2), 183–194.
Mastellos, D.C., et al., 2022. From discovery to approval: a brief history of the compstatin family of complement C3 inhibitors. Clin. Immunol. 235, 108785.
Masuda, T., et al., 2012. IRF8 is a critical transcription factor for transforming microglia into a reactive phenotype. Cell Rep. 1 (4), 334–340.
Mathern, D.R., Heeger, P.S., 2015. Molecules great and small: the complement system. Clin. J. Am. Soc. Nephrol. 10 (9), 1636–1650.
Mattos-Silva, P., et al., 2020. Pros and cons of corticosteroid therapy for COVID-19 patients. Respir. Physiol. Neurobiol. 280, 103492.
McArthur, S., et al., 2016. The restorative role of annexin A1 at the blood-brain barrier. Fluids Barriers CNS 13 (1), 17.
Money, B., et al., 2020. Mechanically adaptive implants fabricated with poly(2-hydroxy¬ethyl methacrylate)-based negative photoresists. J. Mater. Chem. B.
Morgan, B.P., 2018. Complement in the pathogenesis of alzheimer's disease. Semin. Immunopathol. 40 (1), 113–124.
Muller, J., et al., 2015. High-resolution CMOS MEA platform to study neurons at subcellular, cellular, and network levels. Lab Chip 15 (13), 2767–2780.
Nguyen, J.K., et al., 2014. Mechanically-compliant intracortical implants reduce the neuroinflammatory response. J. Neural Eng. 11, 056014.
Nguyen, J.K., et al., 2016. Influence of resveratrol release on the tissue response to mechanically adaptive cortical implants. Acta Biomater. 29, 81–93.
Nilsson, B., et al., 2007. The role of complement in biomaterial-induced inflammation. Mol. Immunol. 44 (1–3), 82–94.
Nolta, N.F., et al., 2015. BBB leakage, astrogliosis, and tissue loss correlate with silicon microelectrode array recording performance. Biomaterials 53, 753–762.
Nonaka, M., Yoshizaki, F., 2004. Evolution of the complement system. Mol. Immunol. 40 (12), 897–902.
Noreen, S., Maqbool, I., Madni, A., 2021. Dexamethasone: therapeutic potential, risks, and future projection during COVID-19 pandemic. Eur. J. Pharmacol. 894, 173854.
Oakes, R.S., et al., 2018. An astrocyte derived extracellular matrix coating reduces astrogliosis surrounding chronically implanted microelectrode arrays in rat cortex. Biomaterials 154, 1–11.
Obien, M.E., et al., 2014. Revealing neuronal function through microelectrode array recordings. Front. Neurosci. 8, 423.
Orsini, F., et al., 2014. Versatility of the complement system in neuroinflammation, neurodegeneration and brain homeostasis. Front. Cell. Neurosci. 8, 380.
Pandarinath, C., et al., 2017. High performance communication by people with paralysis using an intracortical brain-computer interface. Elife 6, e18554.
Park, Y.S., et al., 2020. Early detection of human epileptic seizures based on intracortical microelectrode Array signals. IEEE Trans. Biomed. Eng. 67 (3), 817–831.
Paulk, A.C., et al., 2022. Large-scale neural recordings with single neuron resolution using neuropixels probes in human cortex. Nat. Neurosci. 25 (2), 252–263.
Pfluger, P., et al., 2019. Chronically implanted microelectrodes cause c-fos expression along their trajectory. Front. Neurosci. 13, 1367.

Potter, K.A., et al., 2012. Stab injury and device implantation within the brain results in inversely multiphasic neuroinflammatory and neurodegenerative responses. J. Neural Eng. 9 (4), 046020.
Potter, K.A., et al., 2013. The effect of resveratrol on neurodegeneration and blood brain barrier stability surrounding intracortical microelectrodes. Biomaterials 34 (29), 7001–7015.
Potter-Baker, K.A., et al., 2015. Implications of chronic daily anti-oxidant administration on the inflammatory response to intracortical microelectrodes. J. Neural Eng. 12 (4), 046002.
Proix, T., et al., 2019. Intracortical neural activity distal to seizure-onset-areas predicts human focal seizures. PLoS One 14 (7), e0211847.
Purcell, E.K., et al., 2009. Flavopiridol reduces the impedance of neural prostheses in vivo without affecting recording quality. J. Neurosci. Methods.
Rapeaux, A.B., Constandinou, T.G., 2021. Implantable brain machine interfaces: first-in-human studies, technology challenges and trends. Curr. Opin. Biotechnol. 72, 102–111.
Ravikumar, M., et al., 2014. The effect of residual endotoxin contamination on the neuroinflammatory response to sterilized intracortical microelectrodes. J. Mater. Chem. B 2, 2517–2529.
Ravikumar, M., et al., 2014. The roles of blood-derived macrophages and resident microglia in the neuroinflammatory response to implanted intracortical microelectrodes. Biomaterials S0142–9612 (35), 8049–8064.
C. Rawat, S.K., U. Ranjan Dahiya, R. Kukreti, Cyclooxygenase-2 (COX-2) inhibitors: future therapeutic strategies for epilepsy management. Journal of Neuroinflammation, 2019. 16: p. 197.
Rennaker, R.L., et al., 2007. Minocycline increases quality and longevity of chronic neural recordings. J. Neural Eng. 4 (2), L1–L5.
Riegger, T., et al., 2009. Immune depression syndrome following human spinal cord injury (SCI): a pilot study. Neuroscience 158 (3), 1194–1199.
Rodgers, K.A., et al., 2022. Immune dysfunction after spinal cord injury - a review of autonomic and neuroendocrine mechanisms. Curr. Opin. Pharmacol. 64, 102230.
Saxena, T., et al., 2013. The impact of chronic blood–brain barrier breach on intracortical electrode function. Biomaterials 34 (20), 4703–4713.
Schroeder, K.E., Chestek, C.A., 2016. Intracortical brain-machine interfaces advance sensorimotor neuroscience. Front. Neurosci. 10.
Shoffstall, A.J., et al., 2018. Potential for thermal damage to the blood-brain barrier during craniotomy: implications for intracortical recording microelectrodes. J. Neural Eng. 15 (3), 034001.
Simeral, J.D., et al., 2011. Neural control of cursor trajectory and click by a human with tetraplegia 1000 days after implant of an intracortical microelectrode array. J. Neural Eng. 8 (2), 025027.
Simon, D.M., et al., 2017. Design and demonstration of an intracortical probe technology with tunable modulus. J. Biomed. Mater. Res. A 105 (1), 159–168.
Song, S., et al., 2022. Neuroinflammatory gene expression analysis reveals pathways of interest as potential targets to improve the recording performance of intracortical microelectrodes. Cells 11 (15).
Song, S., et al., 2023. Differential expression of genes involved in the chronic response to intracortical microelectrodes. Acta Biomater. 169, 348–362.
Song, S., Bedell, H.W., Regan, B.J., Ereifej, E.S., Chan, R., Capadona, J.R., 2022. Neuroinflammatory Gene Expression Analysis Reveals Pathways of Interest as Potential Targets to Improve the Recording Performance of Intracortical Microelectrodes. Cells 11 (15), 2348.
Spataro, L., et al., 2005. Dexamethasone treatment reduces astroglia responses to inserted neuroprosthetic devices in rat neocortex. Exp. Neurol. 194 (2), 289–300.
Sridharan, A., et al., 2015. Compliant intracortical implants reduce strains and strain rates in brain tissue in vivo. J. Neural Eng. 12 (3), 036002.
Stett, A., et al., 2003. Biological application of microelectrode arrays in drug discovery and basic research. Anal. Bioanal. Chem. 377 (3), 486–495.
Thompson, C.H., et al., 2021. Spatiotemporal patterns of gene expression around implanted silicon electrode arrays. J. Neural Eng. 18 (4).
Tichaczek-Goska, D., 2012. Deficiencies and excessive human complement system activation in disorders of multifarious etiology. Adv. Clin. Exp. Med. 21 (1), 105–114.
Trouw, L.A., Pickering, M.C., Blom, A.M., 2017. The complement system as a potential therapeutic target in rheumatic disease. Nat. Rev. Rheumatol. 13 (9), 538–547.
Jason Peter Twohig, M.I.R., Nuria Gavalda, Emma L. Rees-Taylor, Albert Giralt, Debbie Adams, Simon P. Brooks, Melanie J. Bull, Claudia J. Calder, Simone Cuff, Audrey A. Yong, Jordi Alberch, Alun Davies, Stephen B. Dunnett, Aviva M. Tolkovsky, and Eddie C. Y. Wang, Age-Dependent Maintenance of Motor Controland Corticostriatal Innervation by Death Receptor 3. J Neurosci, 2010. 30(10): p. 3782-3792.
Usoro, J., et al., 2021. On the definition of 'chronic' for intracortical microelectrode array applications. Micromachines 12 (8), 972.
Vignesh, P., et al., 2017. Complement in autoimmune diseases. Clin. Chim. Acta 465, 123–130.
Wang, Z.M., et al., 2020. SerpinA3N deficiency deteriorates impairments of learning and memory in mice following hippocampal stab injury. Cell Death Discov. 6 (1), 88.
Ware, T., et al., 2012. Fabrication of responsive, softening neural interfaces. Adv. Funct. Mater. 22 (16), 3470–3479.
Welle, E.J., et al., 2020. Ultra-small carbon fiber electrode recording site optimization and improved in vivo chronic recording yield. J. Neural Eng. 17 (2), 026037.
Wells, J.E., et al., 2003. An adverse role for matrix metalloproteinase 12 after spinal cord injury in mice. J. Neurosci. 23 (31), 10107–10115.
Wilhelmsson, U., et al., 2019. The role of GFAP and vimentin in learning and memory. Biol. Chem. 400 (9), 1147–1156.
Willett, F.R., et al., 2021. High-performance brain-to-text communication via handwriting. Nature 593 (7858), 249–254.
Xi, Y., et al., 2019. Inhibition of SERPINA3N-dependent neuroinflammation is essential for melatonin to ameliorate trimethyltin chloride-induced neurotoxicity. J. Pineal Res. 67 (3), e12596.
Yeo, H.G., et al., 2019. Increased CD68/TGFbeta co-expressing microglia/ macrophages after transient middle cerebral artery occlusion in rhesus monkeys. Exp. Neurobiol. 28 (4), 458–473.
Zamanian, J.L., et al., 2012. Genomic analysis of reactive astrogliosis. J. Neurosci. 32 (18), 6391–6410.
Zattoni, M., et al., 2022. Serpin signatures in prion and alzheimer's diseases. Mol. Neurobiol. 59 (6), 3778–3799.
Zhang, Y., et al., 2013. Autonomic dysreflexia causes chronic immune suppression after spinal cord injury. J. Neurosci. 33 (32), 12970–12981.
Zhang, Y., et al., 2022. SerpinA3N attenuates ischemic stroke injury by reducing apoptosis and neuroinflammation. CNS Neurosci. Ther. 28 (4), 566–579.
Zhang, X., et al., 2022. Changes of IL-6 and IFN-gamma before and after the adverse events related to immune checkpoint inhibitors: a retrospective study. Medicine (Baltimore) 101 (46), e31761.
Zhang, J., et al., 2022. The role of lipocalin 2 in brain injury and recovery after ischemic and hemorrhagic stroke. Front. Mol. Neurosci. 15, 930526.
Zheng, N., et al., 2022. CD84 is a suppressor of T and B cell activation during mycobacterium tuberculosis pathogenesis. Microbiol. Spectr. 10 (1), e0155721.
Zhong, Y., Bellamkonda, R.V., 2007. Dexamethasone-coated neural probes elicit attenuated inflammatory response and neuronal loss compared to uncoated neural probes. Brain Res. 1148, 15–27.